2014-12

Implementation of optimal controls using conventional control systems

Arledge, Richard K.

Monterey, California: Naval Postgraduate School

NAVAL POSTGRADUATE SCHOOL

MONTEREY, CALIFORNIA

THESIS

IMPLEMENTATION OF OPTIMAL CONTROLS USING CONVENTIONAL CONTROL SYSTEMS

by

Richard K. Arledge

December 2014

Thesis Co-Advisors: Mark Karpenko
I. Michael Ross

Approved for public release; distribution is unlimited

THIS PAGE INTENTIONALLY LEFT BLANK

REPORT DOCUMENTATION PAGE

Form Approved OMB No. 0704–0188

1. AGENCY USE ONLY *(Leave blank)*	**2. REPORT DATE** December 2014	**3. REPORT TYPE AND DATES COVERED** Master's Thesis

4. TITLE AND SUBTITLE
IMPLEMENTATION OF OPTIMAL CONTROLS USING CONVENTIONAL CONTROL SYSTEMS

5. FUNDING NUMBERS

6. AUTHOR(S) Richard K. Arledge

7. PERFORMING ORGANIZATION NAME(S) AND ADDRESS(ES)
Naval Postgraduate School
Monterey, CA 93943–5000

8. PERFORMING ORGANIZATION REPORT NUMBER

9. SPONSORING /MONITORING AGENCY NAME(S) AND ADDRESS(ES)
N/A

10. SPONSORING/MONITORING AGENCY REPORT NUMBER

11. SUPPLEMENTARY NOTES The views expressed in this thesis are those of the author and do not reflect the official policy or position of the Department of Defense or the U.S. Government. IRB Protocol number ____N/A____.

12a. DISTRIBUTION / AVAILABILITY STATEMENT
Approved for public release; distribution is unlimited

12b. DISTRIBUTION CODE

13. ABSTRACT (maximum 200 words)

This thesis investigates the implementation of optimal control solutions for positioning spacecraft antenna using conventional techniques. Conventional maneuvers consider each axis independently and may include artificial limits that reduce the efficiency of the system. These methods allow simple, but generally suboptimal, maneuver design. Multi-body dynamic systems do, however, exhibit coupling effects that can be advantageous for enhancing motion planning. Including coupling effects in the model can reduce energy needed to implement a slew maneuver. For example, previous work demonstrated that optimal control solutions can reduce required slew time for spacecraft antenna maneuvers. This work explores the utility of implementing such optimal trajectories as reference maneuvers using current control schemes. Development and validation of the approach is explored using systems of increasing dynamic complexity. Two methods to match given optimal control profiles using existing control logic were developed and compared against current practice. The developed methods were applied to the results for a double gimbal model and the Tracking Data Relay Satellite. The developed approach allows optimal trajectories to be successfully matched to within 2% position error along the trajectory using less than four conventional maneuvers. These results thus provide a simplified approach for implanting optimal slew maneuvers.

14. SUBJECT TERMS Optimal Slew Maneuvers, Spacecraft, Antenna, Communications Satellite, Multi-body Dynamics, Dynamic Coupling, Optimal Control, Double Gimbal

15. NUMBER OF PAGES 99

16. PRICE CODE

17. SECURITY CLASSIFICATION OF REPORT	**18. SECURITY CLASSIFICATION OF THIS PAGE**	**19. SECURITY CLASSIFICATION OF ABSTRACT**	**20. LIMITATION OF ABSTRACT**
Unclassified	Unclassified	Unclassified	UU

NSN 7540–01–280–5500

Standard Form 298 (Rev. 2–89)
Prescribed by ANSI Std. 239–18

THIS PAGE INTENTIONALLY LEFT BLANK

Approved for public release; distribution is unlimited

IMPLEMENTATION OF OPTIMAL CONTROLS USING CONVENTIONAL CONTROL SYSTEMS

Richard K Arledge
Lieutenant Commander, United States Navy
B.A., Jacksonville State University, 2001
M.S., Naval Postgraduate School, 2008

Submitted in partial fulfillment of the
requirements for the degree of

MASTER OF SCIENCE IN ASTRONAUTICAL ENGINEERING

from the

NAVAL POSTGRADUATE SCHOOL
December 2014

Author: Richard K. Arledge

Approved by: Mark Karpenko
Co-Advisor

I. Michael Ross
Co-Advisor

Garth V. Hobson
Chair, Department of Mechanical and Aerospace Engineering

THIS PAGE INTENTIONALLY LEFT BLANK

ABSTRACT

This thesis investigates the implementation of optimal control solutions for positioning spacecraft antenna using conventional techniques. Conventional maneuvers consider each axis independently and may include artificial limits that reduce the efficiency of the system. These methods allow simple, but generally suboptimal, maneuver design. Multi-body dynamic systems do, however, exhibit coupling effects that can be advantageous for enhancing motion planning. Including coupling effects in the model can reduce energy needed to implement a slew maneuver. For example, previous work demonstrated that optimal control solutions can reduce required slew time for spacecraft antenna maneuvers. This work explores the utility of implementing such optimal trajectories as reference maneuvers using current control schemes. Development and validation of the approach is explored using systems of increasing dynamic complexity. Two methods to match given optimal control profiles using existing control logic were developed and compared against current practice. The developed methods were applied to the results for a double gimbal model and the Tracking Data Relay Satellite. The developed approach allows optimal trajectories to be successfully matched to within 2% position error along the trajectory using less than four conventional maneuvers. These results thus provide a simplified approach for implanting optimal slew maneuvers.

THIS PAGE INTENTIONALLY LEFT BLANK

TABLE OF CONTENTS

LIST OF FIGURES

LIST OF TABLES

THIS PAGE INTENTIONALLY LEFT BLANK

LIST OF ACRONYMS AND ABBREVIATIONS

BVP	boundary value problem
HMC	Hamiltonian Minimization Condition
IVP	initial value problem
ISS	International Space Station
MEO	Medium Earth Orbit
NASA	National Aeronautics and Space Administration
NPS	Naval Postgraduate School
SA	Single Access
STK	Systems Tool Kit
TDRS	Tracking Data Relay Satellite
TRACE	Transition Region and Coronal Explorer
V&V	Verification and Validation

THIS PAGE INTENTIONALLY LEFT BLANK

ACKNOWLEDGMENTS

Producing a research work of this scope is at best a difficult task. My advisors have done their best to keep this from becoming an administrative exercise and for that I thank them. I appreciate the guidance and advice I received from Dr. Mike Ross and Dr. Mark Karpenko throughout the thesis process; in particular, for helping me to find a topic that would meet the academic intent but also provide a product with real-world applications. My classmates also have my gratitude for being available to share and discuss ideas with when one of us got stuck. Finally, thank you to my family for allowing me to have the time required to complete this process and being there when it was time for me to take a break.

THIS PAGE INTENTIONALLY LEFT BLANK

I. INTRODUCTION

A. MOTIVATION

Many space systems in operation today were designed with conservative operational limits. These limits were chosen during the design process for various reasons, such as limiting stress on components or reducing induced disturbances [1]. Some of this conservatism is a result of providing a desired safety margin but, in many cases, these limits are based on simplifications made during system modeling. Historically model reduction was necessary to develop solutions to these complex problems without the aid of computers [2]. Progress in computing power and software provided engineers and scientists the ability to solve multi-body dynamics problems without simplification [3].

Optimal control problems, which attempt to minimize a user defined cost functional, can now easily be solved using home computers for multi-body dynamic systems, such as spacecraft. These techniques have resulted in more efficient maneuver paths as demonstrated in [2, 4] on the International Space Station and Transition Region and Coronal Explorer (TRACE) spacecraft. This idea has also been applied to communication satellite antenna pointing to reduce slew maneuver times and improve customer access [1].

Optimal maneuvers, however, usually require the implementation of a polynomial-based trajectory for the path. Because of simplifications used to facilitate simple problem solutions, many current systems are designed to maneuver along an eigenaxis path [2]. This path represents the shortest angular path between two points but is not, in general, the time-optimal trajectory [5]. Systems designed using such conventional control logic may not be capable of accepting other, polynomial trajectories as inputs, without some kind of software change. Such changes will typically incur some cost and this tends to deter the adoption of more efficient optimal control maneuver paths.

B. THESIS OBJECTIVE AND SCOPE

This thesis seeks to determine the utility of implementing optimal control solutions using current control techniques to mimic the optimal response. If the optimal path can be achieved without requiring a system to accept or process a polynomial solution, the benefits of optimal control can be exploited by a variety of systems with minimal changes. This approach therefore represents an intermediate step between the current state of practice and the future state of the art. An approach for implementing optimal maneuvers using existing control system will make the benefits accessible to numerous applications including optics, antenna pointing, and robotics.

The development of optimal control problems will be discussed to demonstrate the advantages of this process for maneuver development, particularly for multi-body systems. Optimal control problems will be solved using available computer software. Various applicable cases and systems of increasing dynamic complexity will be evaluated. The optimal solution maneuver path will then be approximated using current methods and the performance achieved will be evaluated.

This thesis approaches the concept of implementing optimal control solutions that have been solved *a priori*. Instead of using the existing control logic to plan and implement a linear maneuver, it is assumed that a certain path to the final position is known and is provided to the spacecraft operator. The given profile can then be matched using a sequence of maneuver steps based on the existing trapezoidal motion profile, shown in Figure 1. This approach allows maneuvers to be solved off line and the maneuver parameters stored for later implementation. It is not necessary to solve the maneuver as part of the flight software.

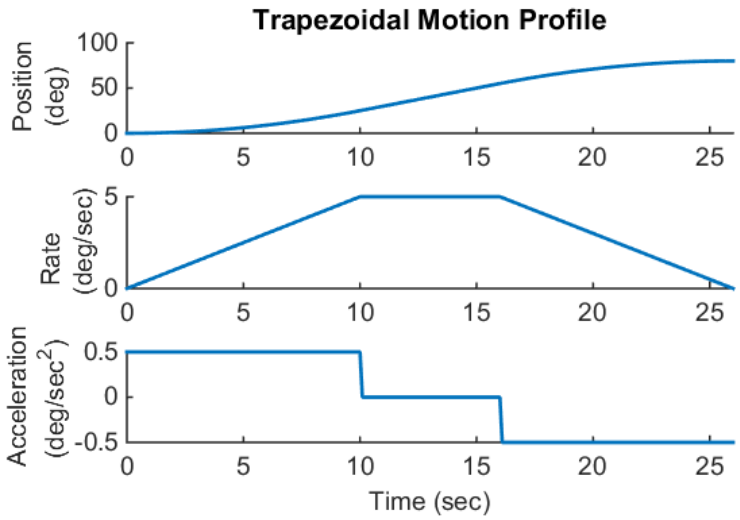

Figure 1. Trapezoidal motion profile.

In the trapezoidal motion profile, the motion has a prescribed maximum acceleration and velocity limit. The maximum acceleration is applied from the initial time until the maximum allowed velocity is reached, then the system coasts at the maximum velocity until near the desired final position. The system then uses negative, full acceleration to return to zero velocity at the desired final position. Torque applied will be constant, only the time of application will be varied to generate the required velocity profile. This is meant to limit the complexity of the implementation to allow the resulting method developed here for inserting optimal motion profiles to be applicable to the widest number of applications.

Finally, the maneuver matching techniques developed will be applied to the Tracking Data Relay Satellite (TDRS), as a practical example. The output of an optimization for TDRS based on the analysis in [1] was used as the optimized path. It is shown that the approach developed in this thesis allows for an optimal solution to be implemented on a real world system using existing control algorithms. The performance of the developed scheme is evaluated by comparing the time required for each sequenced maneuver against the current slew implementation.

C. THESIS OUTLINE

The remainder of this thesis is organized to provide an introduction to optimal control problems, develop the optimal solution matching technique, and then apply the process to selected example cases. Chapter II introduces basic concepts in optimal control theory. Chapter III presents examples of optimal control problems and their solutions. Chapter IV introduces the double gimbal system, describes associated optimization problems, and presents their solutions. Chapter V describes the matching techniques developed for optimal reference paths and provides the results of test case analysis. Chapter VI provides a description of the TDRS optimization problem and presents the results of optimal solution matching technique implementation. Finally, Chapter VII presents conclusions and suggested areas for future work.

II. OPTIMAL CONTROL THEORY

For every operation there is a particular path that represents the minimum resources required to achieve a given goal. Conventionally, the optimum path between two points has been thought to be a straight line. This comes from the idea that the shortest path must represent the best path. It has been shown for multi-body dynamic systems, like spacecraft antennas, that the optimal solution rarely follows a straight line because of the effects of nonlinearities and coupling between the various bodies [6]. The question of what optimal means therefore becomes a relevant piece of information. Generally, operators seek to reduce time, fuel, or torque required to perform a maneuver. In each case, the optimal solution is one that provides the lowest user defined cost to execute the desired action.

Several techniques exist for generating these optimal solutions, each requiring a varying level of user involvement and complexity. These approaches include the formulation of boundary value problems (BVPs), which can be solved in MATLAB using a shooting method or a collocation method or the use of automated computer programs such as DIDO [3, 4]. In this chapter, each of these methods will be briefly discussed.

A. OPTIMAL CONTROL PROBLEMS

An optimal control problem is a set of differential equations that is coupled with a set of boundary conditions and any other constraints on the system with the objective of minimizing a cost functional. The boundary conditions are based on the desired behavior of the system at specific points. These conditions are imposed on the system by fixing the function and some of its derivatives at more than one value of the independent variable [7]. Boundary conditions can be expressed as fixed values or functions. For example, the initial values of position and velocity may be explicitly specified or they may be part of a range of values with the optimal value being dictated by the solution. If boundaries are specified for the entire path of the problem, these conditions force a constraint on the solution [1].

The fundamental optimal control problem, P_C, is given in Equation (2.1) [8].

$$\begin{cases} \text{Minimize} \quad J\left[x(\bullet),u(\bullet),t_f\right] = E\left(x\left(t_f\right),t_f\right) + \int_{t_o}^{t_f} F\left(x(t),u(t),t\right)dt \\ \text{Subject to} \quad \dot{x}(t) = f\left(x(t),u(t),t\right) \\ x\left(t_0\right) = x^0 \\ t_0 = t^0 \\ e\left(x_f,t_f\right) = 0 \end{cases} \tag{2.1}$$

In Equation (2.1), function E represents the endpoint cost in terms of final state and time. Function F represents the running cost based on the state variables, x, a control variable, u, and time, t. Applying Pontryagin's Principle leads to the definition of a BVP, the solution of which provides a solution to P_C.

Pontryagin's Principle is stated as follows: "Given an optimal solution $\left\{x(\bullet),u(\bullet),t_f\right\}$ to Problem P_C, there exists a costate, $\lambda(\bullet)$, and a covector, ν, that satisfies the Adjoint Equation, the Hamiltonian Minimization Condition, the Hamiltonian Value Condition, the Hamiltonian Evolution Equation and the Transversality Condition" [8]. Meeting these conditions does not solve the optimal control problem explicitly, but identifies the required conditions that a candidate optimal solution must satisfy. Each of these conditions will be discussed in relation to the specific example cases used in this thesis.

The first and most important step in the process of solving this type of problem is the problem formulation. To properly formulate an optimal control problem, the three components of P_C above must be present: a function or quantity to minimize, the system dynamics, and a set of boundary conditions and constraints [1]. The problem is constrained and bounded as necessary to limit its scope.

A dynamical model is formulated in state space, given by $\dot{x} = f\left(x,u,t\right)$. This state space model takes the control function *u* as the input and produces response *x*. The next step in the application of Pontryagin's Principle is the development of the Hamiltonian function, *H*, based on the specified problem dynamics. Pontryagin's Principle states that the control function is optimal when *H* is minimized with respect to *u* for all instants in

time [8]. This provides a construct to find the optimal solution to a stated problem, if the control trajectory that minimizes the Hamiltonian can be found.

The Hamiltonian is defined in Equation (2.2).

$$H(\lambda, x, u, t) = F(x, u, t) + \lambda^T f(x, u, t) \tag{2.2}$$

In Equation (2.2), λ represents the adjoint covector, a Lagrange multiplier function, which shadows the established state dynamics, and satisfies the conditions of the adjoint equation [8]:

$$-\dot{\lambda} = \frac{\partial H}{\partial x} \tag{2.3}$$

The adjoint forms a Hamiltonian pair with the state dynamics and minimizing this with respect to u produces a candidate optimal solution. This is known as the Hamiltonian Minimization Condition (HMC) [8].

$$\begin{cases} \underset{u}{\text{Minimize}} \quad H(\lambda, x, u, t) \\ \text{Subject to} \quad u \in \mathbb{U} \end{cases} \tag{2.4}$$

If there are no constraints on the controls, the HMC reduces to the Euler-Lagrange equation and the control that minimizes the Hamiltonian is given by:

$$\frac{\partial H}{\partial u} = 0 \tag{2.5}$$

At this point, there may not be enough information to develop a unique solution to the system of equations because there could be too many unknown quantities. Upon application of Pontryagin's Principles, a system of $2N$ variables, N states, N costates, and $2N$ differential equations is obtained. Thus, knowledge of $2N$ point conditions is necessary to generate a unique solution [1]. All of these point conditions will not necessarily be known at the time the problem is formulated but can be obtained based on the defined system parameters. Other boundary condition information is determined from the terminal Transversality Condition,

$$\lambda\left(t_f\right)=\frac{\partial\overline{E}}{\partial x_f} \tag{2.6}$$

where $\overline{E}$ is the Endpoint Lagrangian.

$$\overline{E}\left(\nu,x_f,t_f\right)=E\left(x_f,t_f\right)+\nu^T e\left(x_f,t_f\right) \tag{2.7}$$

In Equation (2.7), $E\left(x_f,t_f\right)$ represents the endpoint cost, ν is a vector of Lagrange multipliers, one for each endpoint condition, e. Developing the Transversality Condition will introduce N_x new equations, but will also provide N_e unknowns. This allows for the discovery of N_x-N_e additional boundary conditions [8]. In the event that all the states had endpoint conditions explicitly provided in the problem formulation, evaluation of Equation (2.6) would not provide any additional information because all of the $2N$ point conditions necessary would already be known.

Finally, if a specific end time is not required or specified, the Hamiltonian Value Condition must also be introduced and evaluated to provide the final point condition on the Hamiltonian. This would not be required when the final time is specified. The Hamiltonian Value Condition is [8]:

$$H\left[t_f\right]=-\frac{\partial\overline{E}}{\partial t_f} \tag{2.8}$$

Equations (2.2)–(2.8) provide the complete set of equations and boundary conditions required to obtain a unique candidate solution to an optimal control BVP. It should also be noted that slight changes in the boundary conditions of a BVP can lead to significant changes in the behavior of the solution [7]. There are also some cases where required constraints produce additional terms in the Hamiltonian making the simple Euler-Lagrange Equations (2.5) no longer applicable [1]. In these cases, the partial derivative $\partial H/\partial u$ must be interpreted as a switching function.

B. SOLVING AN OPTIMAL CONTROL PROBLEM

Once a BVP has been developed by the application of Pontryagin's Principle, it must be solved. Obtaining a solution to a BVP means to solve the underlying differential equations and satisfy the specified boundary conditions [7]. Numerous techniques exist for solving BVPs. These range from user defined code to pre-programed algorithms that act solely based on user inputs. This section is not meant to be an exhaustive survey of these techniques, but some basic ideas are presented to give the reader an appreciation for the most commonly used techniques. Three basic methods will be discussed: shooting, collocation, and the use of the software program DIDO. All of these methods rely on MATLAB for execution and each presents unique challenges and merits to obtaining the solution to an optimal control problem.

1. Shooting Methods

One common approach for solving optimal control problems is the use of a shooting method, which generates the numerical solution of a BVP by integrating a simpler initial value problem (IVP) [9]. An IVP is determined by specifying all the values of a system of differential equations at a single point, i.e., the initial time. Some initial values will be unknown and must be guessed. A shooting method combines the solution of an IVP with the solution of nonlinear algebraic equations required to satisfy the desired boundary conditions [10]. Shooting methods are relatively easy to program and evaluate using modern computer applications; however, fundamental problems with this method remain for all dynamical systems described by BVPs arising from the application of Pontryagin's Principle.

First, there can be instability in the IVP for the system of differential equations. IVP solutions can be sensitive to changes in the initial values while the solution to the BVP is insensitive to changes in specified boundary values [10]. This issue arises because of the "curse of complexity" where the system time constant is small; there is a large horizon or both [8]. Second, most methods using iterative solvers require good starting values for the guessed initial conditions to generate accurate solutions, especially for

nonlinear problems [9]. These problems can be avoided by using a collocation technique instead.

2. Collocation Techniques

Collocation techniques generate solutions to BVPs by employing linear combinations of convenient sets of functions and determining the coefficients required to satisfy the differential equation at certain points [11]. Unlike the shooting method, information at nodes spanning the whole solution interval, including the boundary conditions, are simultaneously taken into account. Essentially, this method satisfies the differential equation at both ends and the midpoint of a specified subinterval [10]. Collocation relies on the solution of systems of linear equations and not IVPs thus eliminating some of the problems associated with shooting methods.

Despite these advantages, collocation is still highly dependent on the quality of the user supplied guess across the initial mesh. Techniques exist in current software to mitigate the effects of poor guess quality, but this remains the hardest part of solving a BVP [10]. Also, this method is not appropriate where high accuracy is required or where the system displays sharp changes in its solution [10].

3. DIDO

While many options exist for solving optimal control problems, the complexity of the mathematics associated and the required knowledge of the system characteristics cause these approaches to become rapidly unreliable in many real world applications. DIDO is a MATLAB-based software package that greatly simplifies the process of reliably solving optimal control problems. This tool takes a basic problem formulation as discussed in Section A consisting of the system dynamics equations and boundary conditions and develops a solution using pseudospectral optimal control theory [3]. Because of the ease of problem formulation, DIDO allows the user to vary parameters and observe their effects on system output. This output includes the controls, states, and covectors allowing for better understanding of the system response and troubleshooting during solution development [1].

DIDO uses MATLAB as its user interface and requires the specification of four files to formulate the profile and define all necessary variables. These are dynamics, cost, events, and path. The dynamics function provides the differential equations to be optimized and defines the states for each time interval. The cost function describes the endpoint and running cost of the system. These are both user defined and allow for simple analysis of the effects of cost on output. Sometimes this is the most powerful driver of solution variation. The events function provides the known boundary conditions for the basic problem. The path function allows the user to provide additional constraints along the solution path if needed [3]. The path function is considered optional because such constraints are unnecessary for a basic solution.

One additional script is required to call DIDO, a user defined problem definition file. This main problem file defines the number of state variables, the boundaries for the solution space and the number of evaluation points for the system to use. DIDO performs all the analysis of Pontryagin's Principle and develops an extremal solution (a candidate optimal control) as described in Section A. It is possible to use DIDO iteratively by taking the results of the initial solution and using them to seed the next iteration of the solver. This can be done to quickly improve results when high accuracy is required.

To ensure the results are feasible, a verification and validation check must be performed by propagating the DIDO generated control path through the system dynamic equations. This propagation can be done using one of the built in MATLAB ODE tools and a simple comparison graph produced. It is also possible to compare the necessary conditions for optimality (obtained using DIDO) against their expected values (obtained via analysis) to further verify the optimality of the extremal solution. Because of its benefits, DIDO will be used throughout this thesis to solve optimal control problems for test cases examined.

C. SUMMARY

Optimal control problems seek to find a solution to a set of differential equations, subject to boundary conditions, that minimizes a user defined cost function. Applying Pontryagin's Principles to a given optimal control problem produces a BVP which can

then be solved using one of several available methods. Most of these methods are difficult and time consuming to execute by hand, so, computers are used to determine solutions. Even with computer tools some of these methods still present challenges for solution development. DIDO represents a tool for solving these complex problems using only the system dynamics and associated boundary conditions.

The following chapter will explore the use of this tool to develop optimal solutions for a double integrator system. Various cases will be considered through the associated cost function. Resulting optimal paths will be evaluated and compared.

III. SOLVING OPTIMAL CONTROL PROBLEMS USING DIDO

Throughout this thesis, various case studies will be used to illustrate the principles involved in each section. Each system model will be discussed prior to its example case discussion. For the introduction of the theoretical concepts, a simple double integrator system will be used as the test case. This system is simple enough to limit the complexity of the supporting mathematics but complex enough to illustrate the applicable concepts [8].

A. THE DOUBLE INTEGRATOR

The double integrator is a representative dynamic system present in many mechanical system variants including antenna pointing, robotics, and spacecraft maneuvers. Here, the double integrator system is used to represent one axis of a double gimbal system such as the one shown in Figure 2.

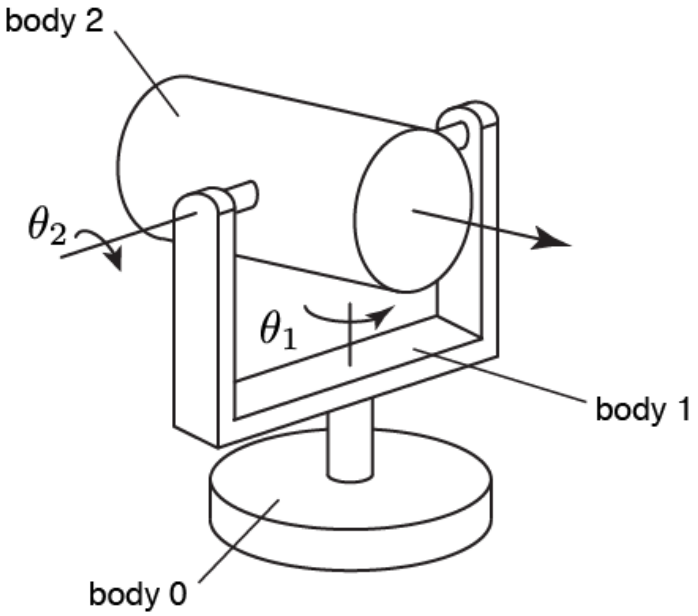

Figure 2. Schematic of a double gimbal system, from [6].

Minimum effort control of the double integrator system is mathematically described in Equation (3.1).

$$x^T = [\theta, \omega] \qquad u = [u] \qquad \mathbb{U} = \mathbb{R}$$

$$\begin{cases} \text{Minimize} & J\left[\theta(\cdot), \omega(\cdot), u(\cdot), t_f\right] = \dfrac{1}{2}\displaystyle\int_0^{t_f} u^2(t)\,dt \\ \text{Subject to} & \dot{\theta} = \omega \\ & \dot{\omega} = u \\ & (\theta_o, \omega_o) = (0,0) \\ & (\theta_f - 1, \omega_f, t_f - 1) = (0,0,0) \end{cases} \tag{3.1}$$

In Equation (3.1), the states are represented by variables $\theta(\cdot)$ and $\omega(\cdot)$ with the control variable represented by $u(\cdot)$. Equation (3.1) presents the simple case of a minimum control effort problem with the cost function based on a quadratic function of the control. This formulation also explicitly gives the initial and final conditions of the state variables and time.

Equation (3.1) is used as the mathematical basis for several optimization problems that vary based on modification of the cost function, states or controls. This very simple system provides a means to explore the results generated by an optimization tool for a maneuver that is intuitive, specifically a transition from point A to point B of one gimbal axis. To illustrate the effects of changes to the problem specifications and to illustrate issues that are applicable to real world problems, results for the following cases will be presented: minimum effort, minimum total maneuver time, rate limited maneuvers, and a multi-objective cost that combines minimum effort and time.

B. MINIMUM EFFORT SOLUTION

To fully describe the minimum effort BVP, the steps discussed in Chapter II.A are applied to transform the problem described by Equation (3.1). This produces the following Hamiltonian.

$$H\left([\lambda_\theta, \lambda_\omega], [\theta, \omega], [u]\right) = \frac{u^2}{2} + \lambda_\theta \omega + \lambda_\omega u \tag{3.2}$$

With the Hamiltonian defined, the five conditions stated in Pontryagin's Principle can each be evaluated to produce an optimal solution to the formulated problem. The first condition is the Hamiltonian Minimization Condition:

$$\frac{\partial H}{\partial u} = 0 \qquad \Rightarrow u + \lambda_{\omega} = 0 \tag{3.3}$$

Equation (3.3) provides a function for the control variable given in terms of the costates.

$$u = -\lambda_{\omega} \tag{3.4}$$

Next, the adjoint equations are evaluated.

$$\begin{aligned} -\dot{\lambda}_{\theta} = \frac{\partial H}{\partial \theta} &= 0 \qquad \Rightarrow \lambda_{\theta} = a, \\ -\dot{\lambda}_{\omega} = \frac{\partial H}{\partial \omega} &= \lambda_{\theta} \qquad \Rightarrow \lambda_{\omega} = -at - b \end{aligned} \tag{3.5}$$

Because of the information already known about the boundary conditions from the problem statement, i.e., all the conditions on the state are given, evaluation of the Transversality and Hamiltonian Value Conditions does not provide new information and the results of these steps are omitted. Using the relationship $u = at + b$ derived from Equations (3.4) and (3.5), the extremal states can be obtained as:

$$\begin{aligned} \omega(t;a,b) &= \frac{at^2}{2} + bt + c \\ \theta(t;a,b) &= \frac{at^3}{6} + \frac{bt^2}{2} + ct + d \end{aligned} \tag{3.6}$$

Using the given boundary conditions the unknown constants in Equation (3.6) can be determined, resulting in the following: $a = -12, \quad b = 6, \quad c = 0, \quad$ and $\quad d = 0$.

A solution satisfying all of the conditions outlined above will be an optimal solution to the problem described by (3.1). Several methods exist to meet these criteria and thus obtain the solution to the BVP for the given conditions. But, as discussed in Chapter II Section B these methods each present their own difficulties. Even a simple system such as the one described by Equation (3.1) can be difficult to solve by hand (as

was done above) if iteration or variation of the problem, such as adding a rate constraint, is desired.

To simplify the determination of the solution, DIDO software can be used. To solve the problem using DIDO, the problem statement of Equation (3.1) is the only item required. In addition to the boundary conditions given in Equation (3.1), bounds are placed on the states, control, and time. These bounds, given in Table 1, are necessary to numerically limit the search space, but are not intended to actively constrain the system response.

Table 1. Box constraints for solving the double integrator problem in DIDO.

Bound	θ	ω	u	t
Lower	-2	-2	-10	0
Upper	2	2	10	1

After formatting the input as discussed in Chapter II Section B, DIDO automatically determines all the conditions required by Pontryagin's Principle. Figure 3 provides graphs of the states, costates, and control values associated with the solution. The solution is consistent with the analytic solution developed in Equations (3.2)–(3.6).

In Figure 3, the states are overlaid with the results of a MATLAB ODE45 propagation of the generated control values through the system dynamics. This provides a method of verification and validation (V&V) of the results produced by DIDO. Furthermore, the Hamiltonian should be a constant with respect to time and take on the value of $-\lambda_v^2/2+\lambda_x v$. Note that since v is unknown, the value of the constant is also unknown. Figure 4 plots the Hamiltonian and demonstrates the expected constancy with a value of $H=-18$.

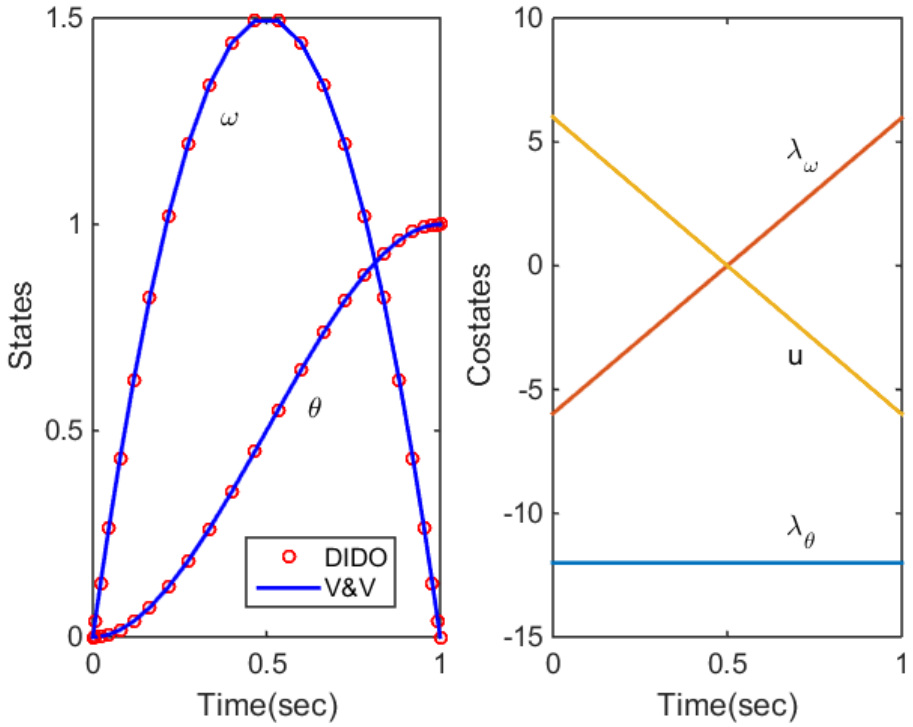

Figure 3. Extremal states, costates, and control for minimum effort double integrator problem.

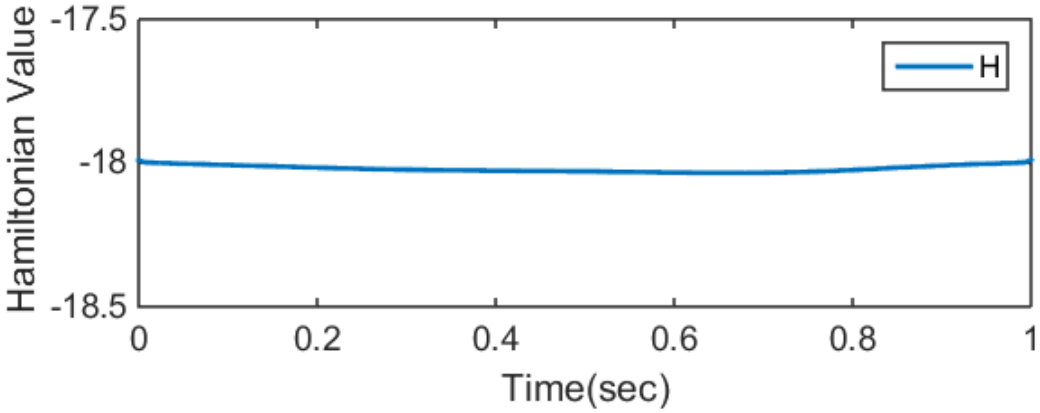

Figure 4. Hamiltonian of minimum effort solution for double integrator problem.

C. MINIMUM TIME SOLUTION

To demonstrate how much a small change in boundary conditions or cost function definition can affect the solution to an optimal control problem, the same dynamic system

is evaluated with the transfer time, t_f , as the cost function. This represents the case of a system operator desiring travel from point A to point B in the least time. Equation (3.7) provides the problem statement for this version of the optimal control problem. Note that the cost function (J) has been changed and the final time left unspecified while all other boundary conditions and relationships remain the same as the previous example.

$$
\begin{aligned}
&x^T = [\theta, \omega] \qquad u = [u] \qquad \mathbb{U} = \{u : |u| \le 10\} \\
&\begin{cases}
\text{Minimize} & J[\theta(\cdot), \omega(\cdot), u(\cdot), t_f] = t_f \\
\text{Subject to} & \dot{\theta} = \omega \\
& \dot{\omega} = u \\
& (\theta_o, \omega_o) = (0,0) \\
& (\theta_f - 1, \omega_f) = (0,0)
\end{cases}
\end{aligned}
\tag{3.7}
$$

The change to the system cost function produces changes in several of the conditions necessary to satisfy Pontryagin's Principle despite the fact that the system dynamics remain the same. Because a final time is not specified, essential information required for the evaluation of the solution is missing. The evaluation of the Transversality and Hamiltonian Value conditions is necessary to obtain the missing information [8].

Differences can be seen starting with the formulation of the system Hamiltonian, which is given by:

$$
H([\lambda_\theta, \lambda_\omega], [\theta, \omega], [u]) = \lambda_\theta \omega + \lambda_\omega u \tag{3.8}
$$

Since the control now appears linearly in the Hamiltonian, the value of the control is not given by the Euler-Lagrange equation since $\partial H / \partial u = 0$ yields $\lambda_\omega = 0$. Now the minimization of the Hamiltonian must be performed subject to the limits on u as in Equation (3.9) [8].

$$
\begin{cases}
\underset{u}{\textit{Minimize}} & H(\lambda, \theta, \omega) = \lambda_\theta \omega + \lambda_\omega u \\
\textit{Subject to} & u \in \mathbb{U} = \{u \in \mathbb{R} : -10 \le u \le 10\}
\end{cases}
\tag{3.9}
$$

Introducing an additional costate, μ, produces the Lagrangian, $\bar{H}$, in Equation (3.10).

$$\bar{H}(\mu,\lambda,\theta,\omega)=\lambda_\theta\omega+\lambda_\omega u+\mu u \tag{3.10}$$

Applying the minimization conditions to $\bar{H}$ now results in $\partial H/\partial u=\lambda_\omega+\mu=0$, which provides the basis for a control switching function.

$$u(\lambda_\omega(t))=\begin{cases}-10 & \text{if} \quad \lambda_\omega(t)\geq 0\\ \\ 10 & \text{if} \quad \lambda_\omega(t)<0\end{cases} \tag{3.11}$$

The resulting adjoint equations remain unchanged. From the given final conditions, the end-point Lagrangian also changes and is given as:

$$\bar{E}(\theta_f,t_f)=\nu_1(\theta_f-1)+\nu_2\omega_f+t_f \tag{3.12}$$

The terminal Transversality Conditions are:

$$\begin{aligned}\lambda_\theta(t_f)=\frac{\partial\bar{E}}{\partial\theta_f} &= \nu_1,\\ \lambda_\omega(t_f)=\frac{\partial\bar{E}}{\partial\omega_f} &= \nu_2\end{aligned} \tag{3.13}$$

The Transversality Conditions do not yield new information about the boundaries but the evaluation of the Hamiltonian Value Condition given in Equation (3.14) does.

$$H\left[t_f\right]=-\frac{\partial\bar{E}}{\partial t_f}=-1 \tag{3.14}$$

As per Equation (3.14), the specific constant Hamiltonian value of -1 is expected for the time optimal solution. In addition, the control acts in a Bang-Bang fashion either being fully on in the positive or negative directions [8]. This simple change to the cost definition presents significant changes to the problem solution development.

Again DIDO was used to solve the optimal control problem. Note that changing the problem in DIDO only required a modification of the cost file. Results are presented in Figure 5. Costates were multiplied by a factor of five to enhance the detail.

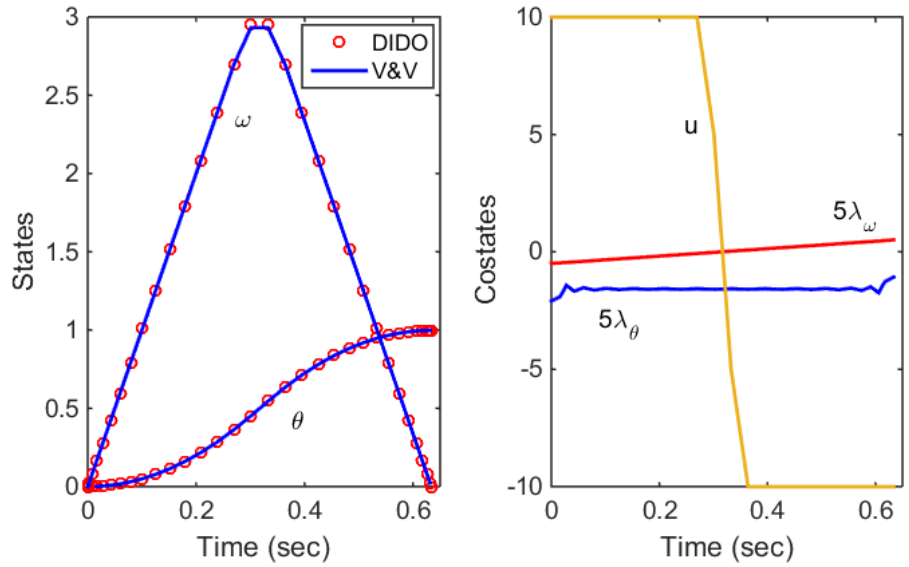

Figure 5. Extremal states, costates, and control for minimum time double integrator problem.

The overall maneuver time was 0.6 seconds and the maximum control authority is used. Reducing the control effort would require a longer time horizon which is why $t_f = 1$ was used in Equation (3.1) for the minimum effort problem. While the motion profile is qualitatively similar to the previous case, the control profile is very different leading to a much higher peak velocity. In this case, the optimal path uses the maximum control effort to generate a larger angular rate in order to reduce the total maneuver time. The control switch point is determined by the costate relationship in Equation (3.11). This response displays the behavior of common Bang-Bang (On-Off) control techniques, where control effort is limited to $u_{\max}$ and $u_{\min}$ only [12]. This minimum time solution can therefore be chosen to simplify maneuver design for complex dynamic systems.

Figure 6 shows the DIDO output for the Hamiltonian of the time optimal maneuver of a single gimbal axis. The Hamiltonian value in Figure 6 is also much different when time is included in the cost evaluation. For optimal time maneuvers, the Hamiltonian value is expected to be -1 as defined by Equation (3.14). In the numerical results, the small deviation from -1 (around 0.3 seconds) is a numerical artifact caused by the switching from maximum positive control effort to maximum negative control effort.

Nonetheless, the Hamiltonian displays the behavior expected for a valid optimal control solution.

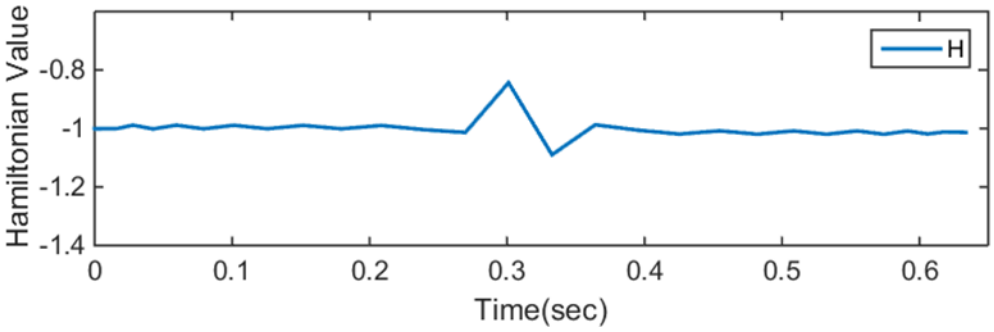

Figure 6. Hamiltonian of minimum time solution for double integrator.

D. RATE LIMITED RESULT

For many applications, rate limits are incorporated for various reasons such as limiting induced disturbances or ensuring safety margins based on material properties. To illustrate the effect that a rate limit has on the optimal solution, the double integrator system was run with the rate limit set at $\pm 1.2\,^{o}/s$, so that the constraint becomes active. The problem formulation and DIDO results for this case will be presented but a complete development of the associated BVPs will be omitted as they are not needed to obtain the solutions.

1. Minimum Effort Solution

The rate limited, minimum effort, double integrator case was formulated as shown in Equation (3.15).

$$x^T = [\theta, \omega] \qquad u = [u] \qquad \mathbb{U} = \mathbb{R}$$

$$\begin{cases} \text{Minimize} & J\left[\theta(\cdot), \omega(\cdot), u(\cdot), t_f\right] = \dfrac{1}{2}\displaystyle\int_0^{t_f} u^2(t)\,dt \\ \text{Subject to} & \dot{\theta} = \omega \\ & \dot{\omega} = u \\ & (\theta_o, \omega_o) = (0,0) \\ & (\theta_f - 1, \omega_f, t_f - 1) = (0,0,0) \\ & -1.2 \le \omega \le 1.2 \end{cases} \tag{3.15}$$

Again, the problem was solved in DIDO and the results were validated using a propagation with ODE45. The Hamiltonian value exhibited the expected constancy and is omitted for brevity. Control and costate behavior was significantly different from the rate free case as seen in Figure 7.

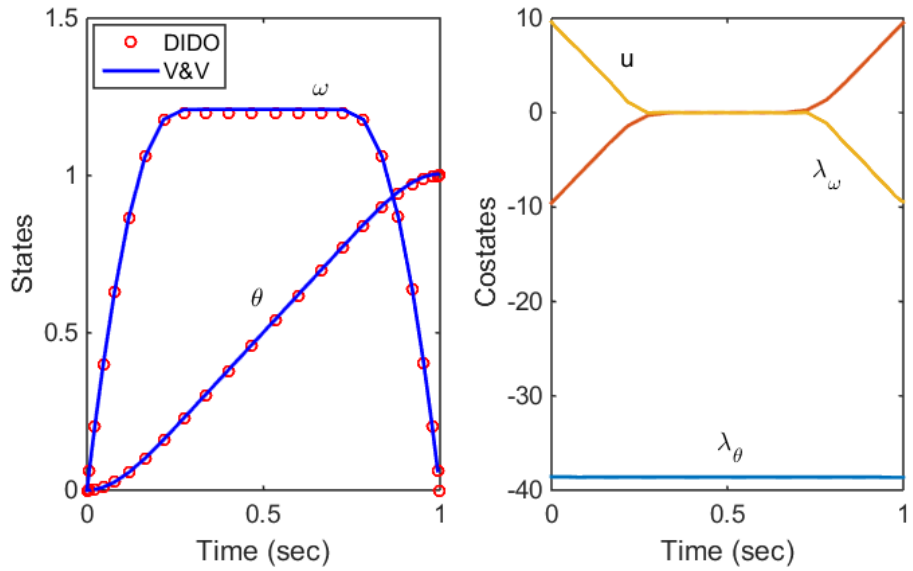

Figure 7. Extremal states, costates, and control for rate limited minimum effort double integrator problem.

With the rate limit in place, the control profile now follows a On-Off-On model. This small and very realistic limitation to the system caused a notable change in the

trajectory of the system. The rate profile is constant at the maximum allowed value for more than half of the maneuver, during which the value of the control is zero.

2. Minimum Time

The problem statement for the rate limited, minimum time, case is presented in Equation (3.16). Note the changes in J and the imposed rate limit based on the minimum time results given in Section C.

$$
\begin{aligned}
&x^T = [\theta, \omega] \qquad u = [u] \qquad \mathbb{U} = \{u : |u| \le 10\} \\
&\begin{cases}
\text{Minimize} & J\left[\theta(\cdot), \omega(\cdot), u(\cdot), t_f\right] = t_f \\
\text{Subject to} & \dot{\theta} = \omega \\
& \dot{\omega} = u \\
& (\theta_o, \omega_o) = (0,0) \\
& (\theta_f - 1, \omega_f) = (0,0) \\
& -1.2 \le \omega \le 1.2
\end{cases}
\end{aligned}
\tag{3.16}
$$

The Hamiltonian value exhibited the expected constant value of -1 and is omitted. Costate behavior was similar to Figure 7 and is also omitted. The DIDO results were validated using the ODE45 method shown here with circle markers. Results for the V&V propagation are presented in Figure 8. Note the total time is greater than the case without the rate limit presented in Section C. The increase in time is a result of the changes in the control and rate profiles that result from the addition of the active rate constraint.

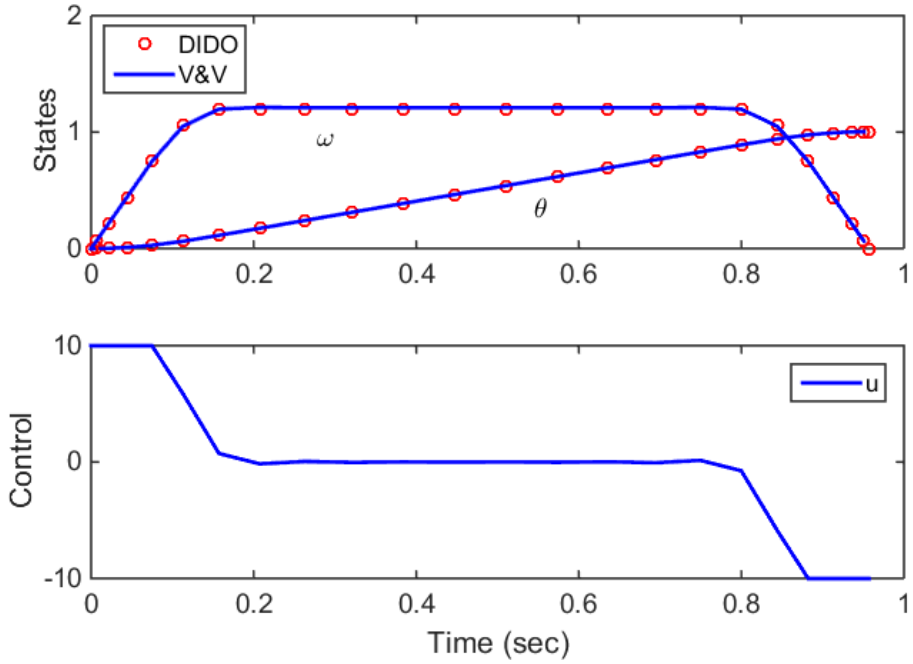

Figure 8. DIDO and V&V results for minimum time rate limited double integrator problem.

The control profile for this time optimal rate limited maneuver follows the Bang-Off-Bang model, while the rate follows a trapezoidal profile. Similar to the Bang-Bang maneuver, the Bang-Off-Bang maneuver is common in many applications due to ease of implementation and ease of modeling system limitations.

E. MULTI-OBJECTIVE RESULTS

There are cases when designers and operators need to minimize more than one parameter at the same time. This is illustrated by constructing a cost function for the double integrator example that considers both the time and effort required. The boundary of the search range for final time was set at five seconds. The problem statement is presented in Equation (3.17).

$$x^T = [\theta, \omega] \qquad u = [u] \qquad \mathbb{U} = \mathbb{R}$$

$$\begin{cases} \text{Minimize} & J\left[\theta(\cdot), \omega(\cdot), u(\cdot), t_f\right] = t_f + \frac{1}{2}\int_0^{t_f} u^2(t)\,dt \\ \text{Subject to} & \dot{\theta} = \omega \\ & \dot{\omega} = u \\ & (\theta_o, \omega_o) = (0,0) \\ & (\theta_f - 1, \omega_f) = (0,0) \\ & -4 \le \omega \le 4 \end{cases} \tag{3.17}$$

Figure 9 displays the DIDO results along with V&V. Because time was included in the cost functional, the Hamiltonian exhibited the constant -1 value associated with a time optimal solution. This case exhibits similar motion and control profiles as those demonstrated in Section B, but it takes just over twice as long to move to the required end state. The addition of the u^2 term to the cost functional produces a much smoother profile than the one displayed in the minimum time results of Section C. It is also possible to apply weighting factors to the cost functional components to emphasize time or effort optimality. The results presented are unweighted, with time and effort contributing equally. Comparing the result of Figure 9 to Figure 3, where the minimum effort problem was solved over a one second time horizon, it is apparent that the control effort is more dominant than the maneuver time in this case.

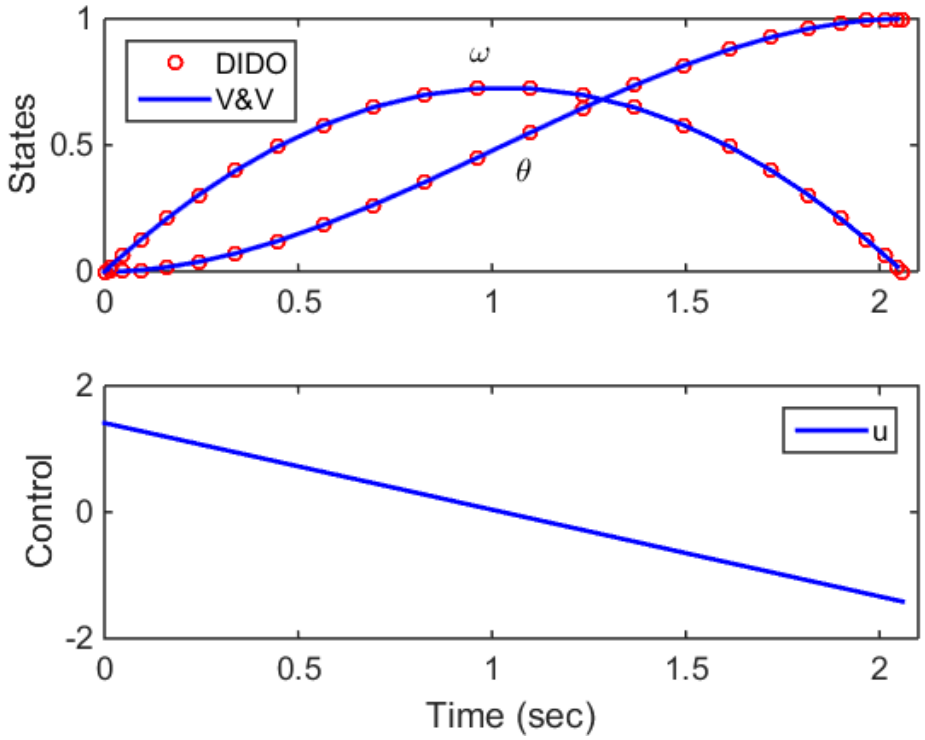

Figure 9. DIDO and V&V results for combined minimum time and effort double integrator problem.

F. SUMMARY

This chapter has shown, through a series of simple examples, that there can be many "optimal" solutions depending on what the designer or user requires from their system, for example rapid slew maneuvers or energy conservation. Each of these cases has a real world application that depends on how the system is employed. Each small change to a boundary condition, cost function, or desired end state can have a large impact on the real-world operation of the system. During this analysis, performance changes of 30–40% in time or effort could be affected by small changes in parameters. Thus, it is highly desirable that a procedure for implementing a variety of optimal control solutions on existing hardware be derived so that operators realize these types of benefits on existing systems.

IV. DOUBLE GIMBAL OPTIMIZATION

The simple double integrator system discussed in Chapter III provides a useful model to illustrate the concepts of optimal control. These ideas can be applied to each individual axis of a system such as the one depicted in Figure 2, however, treating each axis or component individually limits the possible benefits of optimization. This is because kinematic planning leads to inefficiency due to the need to specify conservative bounds on acceleration and velocity which decrease system performance. In multi-body systems, the nonlinear dynamic coupling of the links may be employed by system designers and operators to further enhance performance [6].

It is possible to apply optimal control theory to multi-body systems as a whole in order to leverage the advantages of coupling and nonlinearities and design a motion trajectory accordingly. In this case, the coupling relationships can be used to limit the effects of induced disturbances while simultaneously reducing the time required for maneuvers as compared with traditional approaches [6]. This is a departure from current practice which bases most designed trajectories, particularly for minimum-time motion, on kinematic relationships alone [13].

A. DOUBLE GIMBAL DYNAMICS

Taking nonlinear and coupling terms into account requires deriving the multi-body system dynamics which can rapidly become complicated based on the number of included bodies. Figure 10 gives a schematic of the forces and interactions present in a basic double gimbal such as the one presented in Figure 2. This model can also be used to describe a multi-body satellite system with a gimbaled appendage [1].

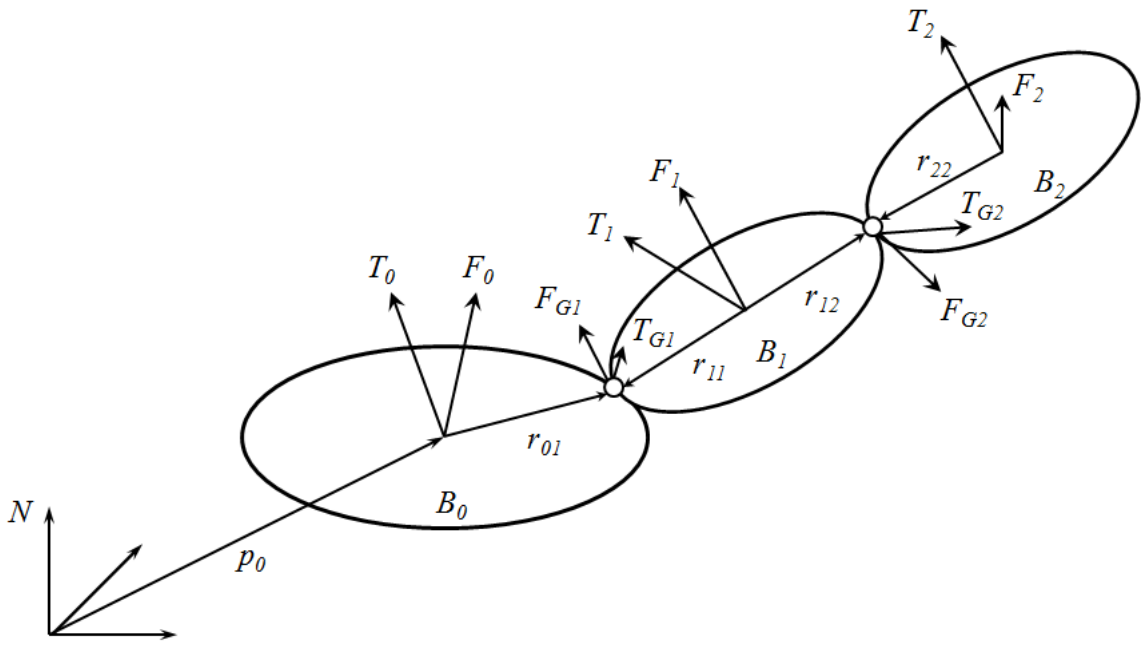

Figure 10. Schematic of a multi-body double gimbal system.

In Figure 10, the base and its forces are represented by body B_0, the azimuth gimbal and its forces by body B_1, and the elevation gimbal and its forces by body B_2. Considering each link as a separate body and describing the joint torques and constraint forces independently of other applied forces, allows for the construction of Newton-Euler equations of motion [14] for any two bodies in the system. Equation (4.1) gives the main result of this analysis.

$$\begin{aligned} I_i\dot{\omega}_i &= T_i - \omega_i \times H_i + T_G + r_i \times F_G \\ I_o\dot{\omega}_o &= T_o - \omega_o \times H_o + T_G + r_o \times F_G \\ m_i\dot{v}_i &= F_i + F_G \\ m_o\dot{v}_o &= F_o + F_G \end{aligned} \tag{4.1}$$

In (4.1), the terms F_G and T_G are the constraint forces and torque at the joint while all other symbols are defined in Table 2.

Table 2. Symbols used in Newton-Euler equations, after [14].

Symbol	Description
ω_i, ω_o	Angular velocity (rad/s)
v_i, v_o	Velocity of mass center (m/s)
I_i, I_o	Central moments of inertia $(kg \cdot m^2)$
m_i, m_o	Mass (kg)
r_i, r_o	Vector from mass center to joint (m)
H_i, H_o	Central angular momentum $(N \cdot m \cdot s)$
F_i, F_o	Resultant external force (N)

The dynamics can become quite complicated with multiple, connected bodies. The model described in Figure 10 along with the necessary coordinate frame transformations require a $6N+3(N-1)$ system of equations, where N is the number of links, to describe three rotational degrees of freedom. It is, therefore, advantageous to eliminate the constraint forces by deriving a set of dynamics equations in the following form [14]:

$$\begin{bmatrix} A & R \\ S & U \end{bmatrix} \begin{Bmatrix} \dot{x} \\ F_G \end{Bmatrix} = \begin{Bmatrix} T' \\ F' \end{Bmatrix} \tag{4.2}$$

This technique allows the dimension of the state vector to be reduced to $3N+3$ by eliminating the joint constraint forces. This means that by using (4.2) for the simple double gimbal depicted in Figure 10, only 12 equations are required to describe the system dynamics rather than 24 if the constraint forces were not eliminated.

For the analysis of this chapter, the element of interest is to observe the effects of dynamic coupling on the optimal trajectory. To this end, additional assumptions and

simplifications were made to reduce the system complexity while preserving the desired interactions. For example, it is assumed the center of mass of each body is aligned with its center of rotation, reducing mass imbalance effects. The center of rotation for each link is coincident with the frame origin and the same point for each. The product of inertia terms are also neglected for simplification. Finally, the system is assumed to provide perfect motion control of the base body. Applying these assumptions yields the following equations of motion [6]:

$$\begin{bmatrix} I_{1zz} + I_{2xx}\sin\left(\theta_2\right)^2 + I_{2zz}\cos\left(\theta_2\right)^2 & 0 \\ 0 & I_{2yy} \end{bmatrix} \begin{bmatrix} \ddot{\theta}_1 \\ \ddot{\theta}_2 \end{bmatrix} = \begin{bmatrix} \tau_1 \\ \tau_2 \end{bmatrix} - \begin{bmatrix} 2\left(I_{2xx} - I_{2zz}\right)\sin\left(\theta_2\right)\cos\left(\theta_2\right)\dot{\theta}_1\dot{\theta}_2 \\ \left(I_{2zz} - I_{2xx}\right)\sin\left(\theta_2\right)\cos\left(\theta_2\right)\dot{\theta}_1^2 \end{bmatrix} \quad (4.3)$$

In (4.3), I is the moment of inertia, θ is the body position, τ is the control torque, and $\dot{\theta}$ is the body rate. Subscripts denote the specific body and, for I, the principle axis associated with the quantity. Coupled motion occurs when $I_{2xx} \neq I_{2zz}$, otherwise, the nonlinear coupling term is eliminated and each gimbal can be rotated independently of the other [15].

B. OPTIMIZATION OF THE DOUBLE GIMBAL SYSTEM

The motion of the double gimbal system was optimized using DIDO for the general three body case. Body zero is the system base, body one the azimuth gimbal, and body two the elevation gimbal. Based on the assumptions made for the system, the resulting responses of body zero were assumed to be precisely controlled and thus ignored. The optimal control problem formulation for the double gimbal system is analogous to the one given in Chapter III, although the dynamics are more complex. Equation (4.4) presents the general optimal control problem statement for the three body case [1].

$$x = \begin{Bmatrix} \omega_0 & \dot{\theta}_1 & \dot{\theta}_2 & v_0 & \theta_1 & \theta_2 & d_1 & q \end{Bmatrix}^T \quad u = \begin{Bmatrix} T_{G1} \\ T_{G2} \end{Bmatrix}$$

Minimize $J = E + \int_{t_0}^{t_f} F dt$

Subject to:

$$\dot{x}' = \frac{d}{dt}\begin{Bmatrix} \omega_0 \\ \dot{\theta}_1 \\ \dot{\theta}_2 \\ v_0 \\ \theta_1 \\ \theta_2 \\ d_1 \\ \begin{Bmatrix} q_1 \\ q_2 \\ q_3 \\ q_4 \end{Bmatrix} \end{Bmatrix} = f(x', u, t) = \begin{Bmatrix} \begin{Bmatrix} (A - RU^{-1}S)^{-1}(T' - RU^{-1}F') \end{Bmatrix} \\ \dot{\theta}_1 \\ \dot{\theta}_2 \\ v_1 \\ \begin{Bmatrix} \frac{1}{2}\begin{bmatrix} q_4 & -q_3 & q_2 & q_1 \\ q_3 & q_4 & -q_1 & q_2 \\ -q_2 & q_1 & q_4 & q_3 \\ -q_1 & -q_2 & -q_3 & q_4 \end{bmatrix}\begin{Bmatrix} \omega 1 \\ \omega 2 \\ \omega 3 \\ 0 \end{Bmatrix} \end{Bmatrix} \end{Bmatrix}$$

$$\begin{Bmatrix} \omega_0(t_0) \\ \dot{\theta}_1(t_0) \\ \dot{\theta}_2(t_0) \\ v_0(t_0) \\ \theta_1(t_0) \\ \theta_2(t_0) \\ d_1(t_0) \\ q(t_0) \end{Bmatrix} = \begin{Bmatrix} [0,0,0]^T \\ [0,0,0]^T \\ [0,0,0]^T \\ [0,0,0]^T \\ [0,0,0]^T \\ [0,0,0]^T \\ [0,0,0]^T \\ [0,0,0,1]^T \end{Bmatrix} \quad \begin{matrix} t_0 = 0 \\ t_f = t^f \end{matrix} \quad \begin{Bmatrix} \theta_1(t_f) \\ \theta_2(t_f) \\ \dot{\theta}_1(t_f) \\ \dot{\theta}_2(t_f) \end{Bmatrix} = \begin{Bmatrix} [\theta_{1xf}, \theta_{1yf}, \theta_{1zf}]^T \\ [\theta_{2xf}, \theta_{2yf}, \theta_{2zf}]^T \\ [\dot{\theta}_{1xf}, \dot{\theta}_{1yf}, \dot{\theta}_{1zf}]^T \\ [\dot{\theta}_{2xf}, \dot{\theta}_{2yf}, \dot{\theta}_{2zf}]^T \end{Bmatrix} \quad u_L < u < u^U \tag{4.4}$$

The problem statement of Equation (4.4) describes orientation of the azimuth gimbal as θ_1 and the elevation gimbal as θ_2. Base rotation and translation are described by ω_o and v_o, respectively with q representing the base attitude in quaternions. The $(A - RU^{-1}S)^{-1}(T' - RU^{-1}F')$ term results from the algebra needed to reduce the dimension of the equations of motion, as in Equation (4.2). The reduction process is described in detail in [1] and [14]. The system inertia tensors used were

$I_1 = diag\left(\left[4,4,6\right]\right) kg \bullet m^2$ and $I_2 = diag\left(\left[2,2,4\right]\right) kg \bullet m^2$. Other relevant constraints are listed in Table 3.

Table 3. Bounds for double gimbal problems.

Bound	$\theta_1 \left(\text{deg}\right)$	$\theta_2 \left(\text{deg}\right)$	$\dot{\theta}_1 , \dot{\theta}_2 \left(\text{deg/sec}\right)$	$u \left(\text{in-oz}\right)$	$t \left(\text{sec}\right)$
Lower	-90	-60	-50	-191	0
Upper	90	60	50	191	25

1. Minimum Time Case

The system of equations in Equation (4.4) was used with the boundary conditions of Table 3 and varying cost functions to investigate the influence of the coupling terms. First, a maneuver from 0^o to 40^o azimuth and 40^o to 20^o elevation was evaluated with the cost function $J = t_f$, yielding the minimum time solution to this optimal control problem. The resulting trajectory is presented in Figure 11 and the resulting Hamiltonian in Figure 12.

Figure 11. Time optimal gimbal trajectories for double gimbal problem.

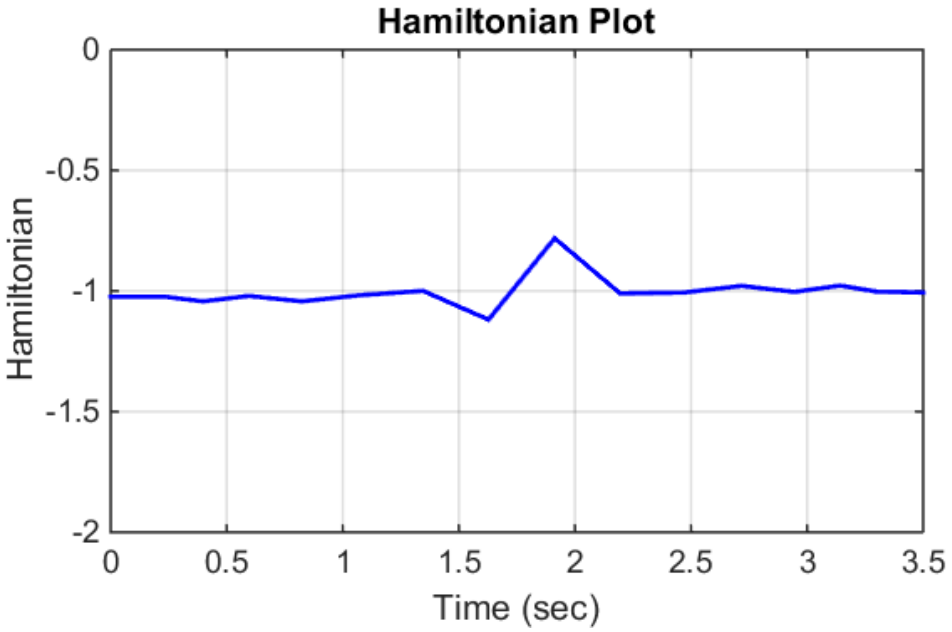

Figure 12. Hamiltonian for time optimal double gimbal problem.

The small variation between the resulting optimal trajectories and the V&V propagation are the result of "open-loop" error that would be corrected by the control system during implementation. The plot of the Hamiltonian, Figure 12, shows the expected value of -1 with slight variation due to numerical artifacts that correlate to the control switching time of the azimuth gimbal. The changes to the profile that result from the inclusion of coupling can be seen in the angle, rate, and torque profiles shown in Figure 13 and Figure 14. Figure 13 presents the resulting angle and rate profile along with the V&V of this output. Figure 14 depicts the torque profile required to produce the motion.

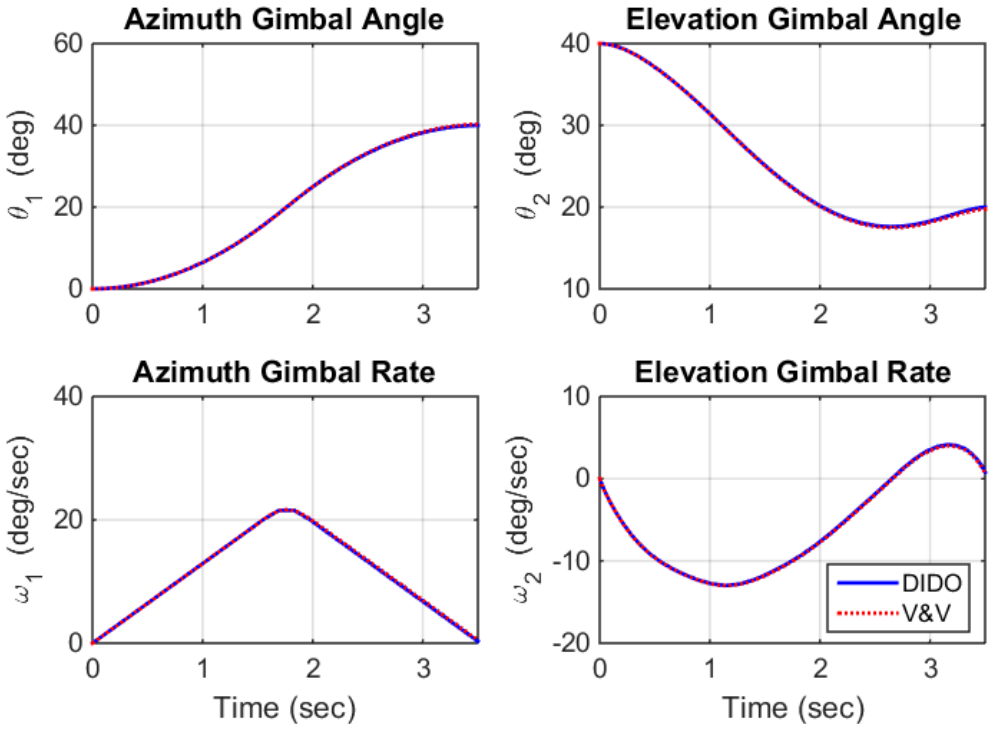

Figure 13. Optimal control results with V&V for time optimal double gimbal problem.

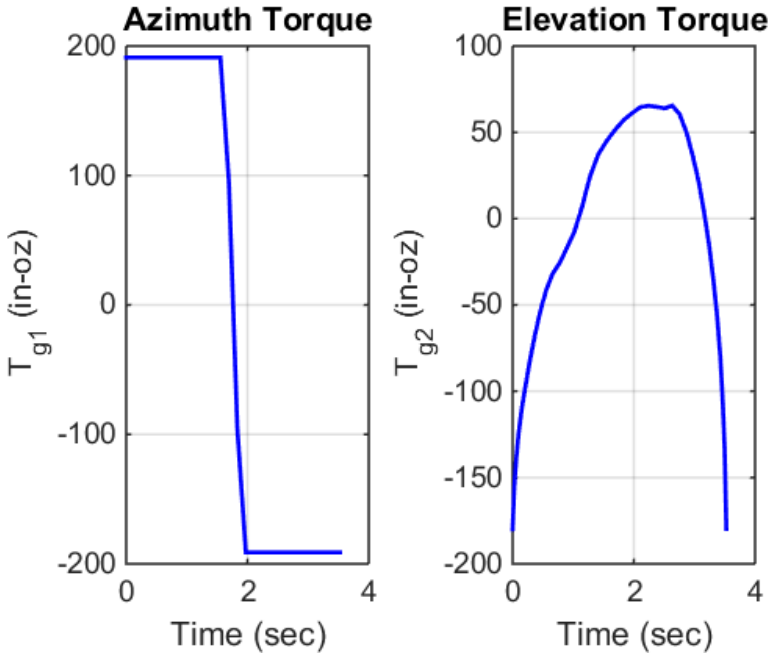

Figure 14. Gimbal torque for time optimal double gimbal problem.

The axis with the larger change in angle, in this case azimuth, is observed to follow a Bang-Bang profile similar to the results obtained in Chapter III.C. The torque profile for the other axis, elevation, generates a non-standard rate and position profile (see Figure 13). The motion of the non-dominant gimbal results, in part, from the torque generated internal to the system as a result of dynamic coupling, given as:

$$\begin{aligned} \tau_{c,AZ} &= 2\left(I_{2xx} - I_{2zz}\right)\sin\left(\theta_2\right)\cos\left(\theta_2\right)\dot{\theta}_1\dot{\theta}_2 \\ \tau_{c,EL} &= \left(I_{2zz} - I_{2xx}\right)\sin\left(\theta_2\right)\cos\left(\theta_2\right)\dot{\theta}_1^2 \end{aligned} \tag{4.5}$$

Figure 15 presents the coupling torque for the minimum time maneuver.

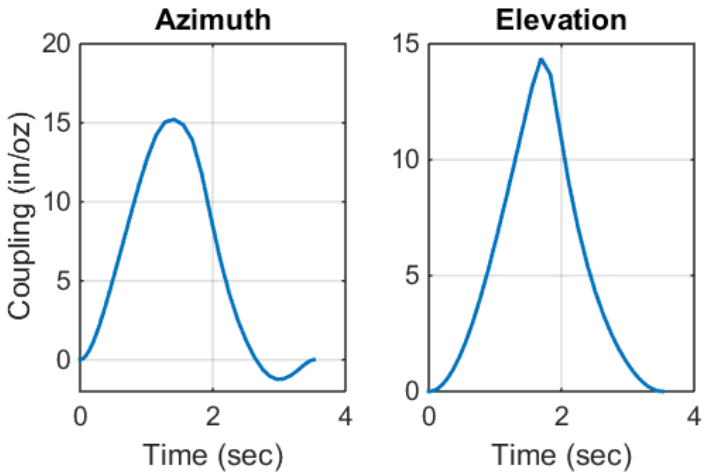

Figure 15. Coupling torque for time optimal double gimbal problem.

Modeling this torque as part of the system and including it, rather than treating it as a disturbance, enhances the capabilities of the system. The same double gimbal minimum time problem with each axis uncoupled (i.e., by setting $I_{2xx} = I_{2zz}$) produces no coupling term and requires additional torque in the elevation axis. Therefore, if coupling effects were not included in the model (kinematic planning), more energy would need to be expended in order to implement a slew between the same two initial and final gimbal orientations.

2. Minimum Effort Case

Optimal control of the double gimbal system was also evaluated using the same boundary conditions and initial and final states as in the minimum time case but with the cost being based on control effort instead. The new cost function is $J = \frac{1}{2}\int_{t_o}^{t_f}\left(T_{G1}^2 + T_{G2}^2\right)dt$.

Here T_{G1} and T_{G2} are the individual gimbal torques of each axis. Also, in order to achieve the minimum maneuver time with the minimum control effort, the upper limit for t_f was bounded to the minimum time of 3.5 seconds, established in the previous case. The solution to this problem results in the trajectory in Figure 16.

Figure 16. Minimum effort trajectory for double gimbal problem.

The Hamiltonian shown in Figure 17 displays the expected behavior, maintaining a constant value. Again, slight variation in the Hamiltonian is seen at the switch point of the control due to numerical effects.

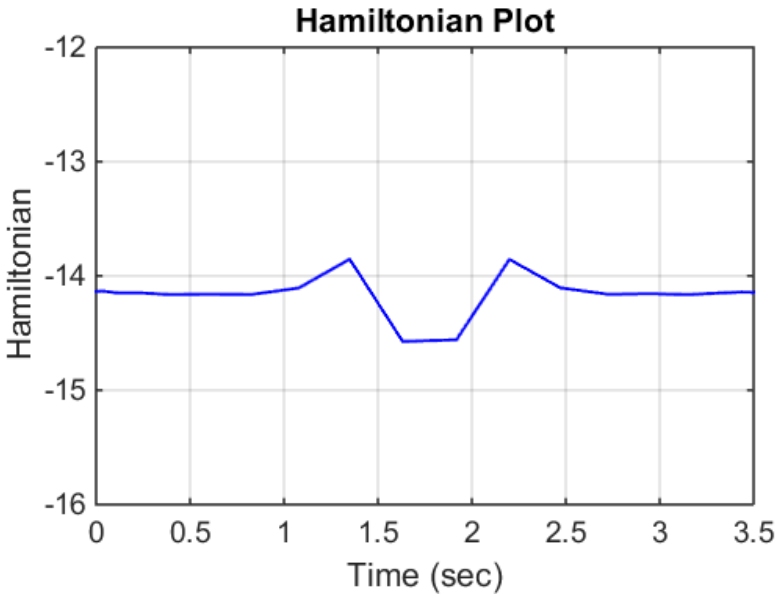

Figure 17. Hamiltonian for minimum effort double gimbal problem.

The gimbal angle and rate results with V&V for each axis are presented in Figure 18. The resulting torque profiles are presented in Figure 19.

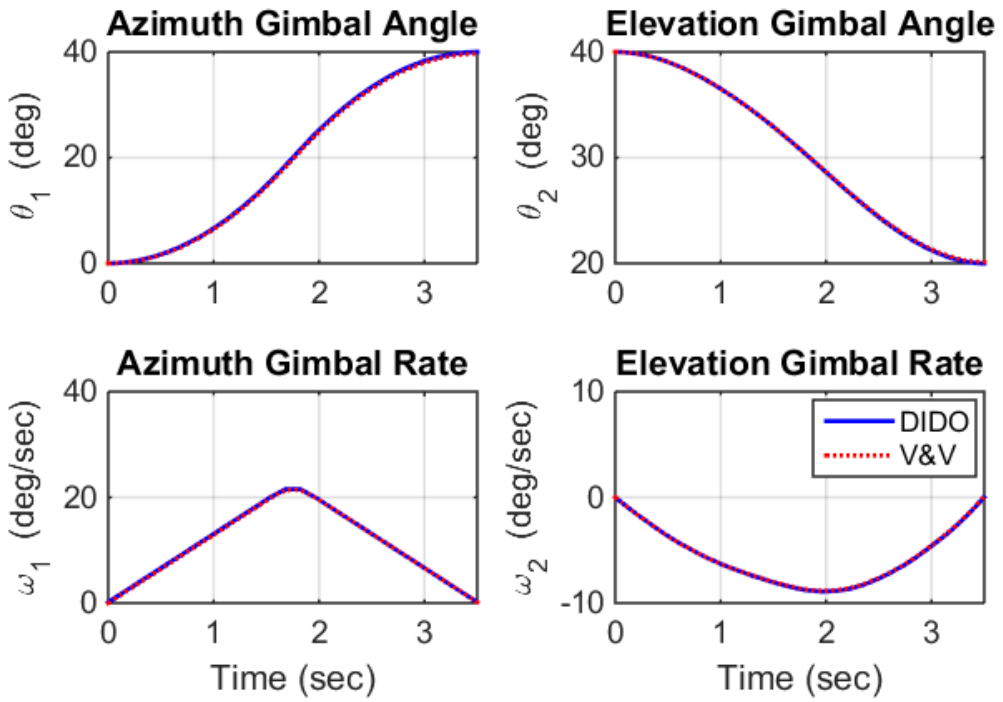

Figure 18. DIDO results with V&V for minimum effort double gimbal problem.

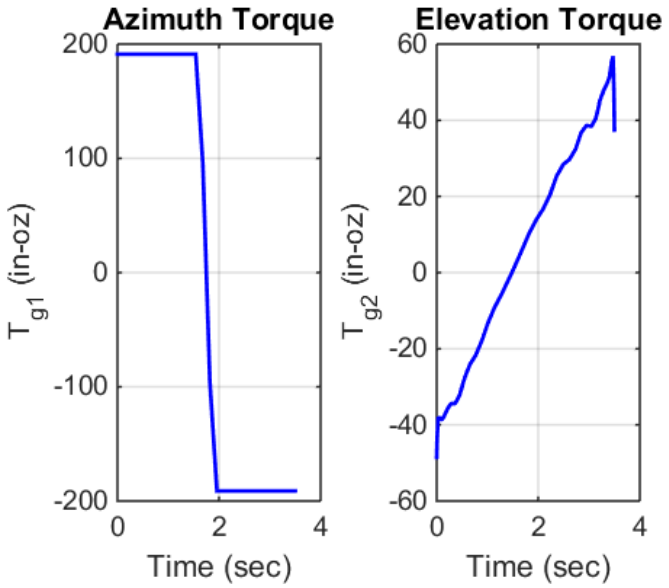

Figure 19. Gimbal control torque for minimum effort double gimbal problem.

The azimuth gimbal, which is the longer of the two maneuvers, still follows the Bang-Bang trajectory. The motion of the elevation gimbal has, however, changed significantly. The profile for elevation angle is nearly the same smooth path as the one for azimuth angle. The torque profile has become a straight line with no abrupt changes and a constant variation as the maneuver progresses. The coupling behavior, shown in Figure 20, is similar to the minimum time case. In this case, however, the coupling torque on the azimuth gimbal has slightly reduced, which enhances the effectiveness of the azimuth gimbal drive.

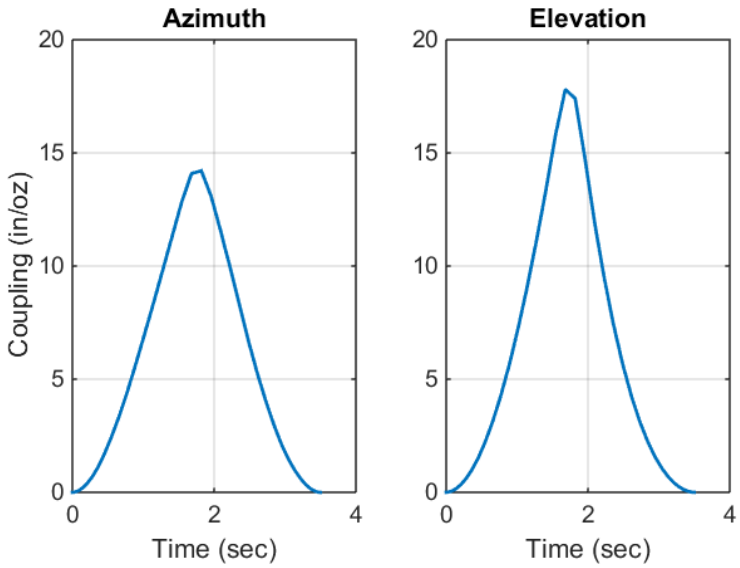

Figure 20. Coupling torque for minimum effort double gimbal problem.

C. SUMMARY

This chapter has applied the principles of optimal control to a more complex system, specifically the double gimbal system. The example problems presented in this chapter illustrate the effects of including higher order dynamic systems on optimal solutions. Using system dynamics, rather than kinematic planning, and including the effects of coupling significantly alter the resulting maneuver paths. The resulting maneuver paths follow polynomial trajectories that existing systems may not be capable of producing.

The next chapter will explore the possibility of reproducing these more complex optimal paths using a sequence of sub-optimal maneuvers. A conventional control implementation using on-off torque input will be modeled. Next, simple maneuver profiles will be broken into steps to ensure the conventional implementation is capable of producing polynomial paths. Finally, an optimal path will be matched using the developed sequence of conventional maneuvers.

THIS PAGE INTENTIONALLY LEFT BLANK

V. MATCHING OPTIMAL REFERENCE PATHS

In order to implement optimal control solutions on current systems it is necessary to understand the methods used to maneuver current systems. The most common approach is to use a bang-bang or a bang-off-bang maneuver. These kinematics based trajectories are the same ones obtained for the minimum time double integrator model described in Chapter III. These types of maneuvers have been employed primarily because they are simple. They are, however, not the most efficient approach for operating a complex dynamic system [1]. As a consequence, the flight software for many space systems is not sophisticated enough to directly accommodate the optimal solution, which, as shown in the previous chapter, is not always a Bang-Bang or Bang-Off-Bang response.

A. CONVENTIONAL CONTROL MODEL

To work towards developing an approach for inserting optimal maneuvers to a conventional system, a basic control implementation for a double gimbal, such as described in Chapter IV, was modeled in MATLAB. This approach represents the typical control implementation generally available on space systems. In this method, each gimbal axis is treated individually for planning purposes. The desired maneuver in each axis is evaluated, based on system capabilities, to determine the time required to complete the maneuver plan.

For this model, it was assumed that both gimbal axes should arrive at their final locations concurrently, similar to TDRS [16]. To achieve this desired condition, the largest time required of either axis was used as the maneuver final time. The maximum velocity of the other, faster axis was reduced to extend the time required for that axis to the maneuver final time. Gimbal acceleration was assumed to be constant and the time applied varied to obtain required velocity values. This is consistent with many applications [16].

This model demonstrates essential elements of the procedure required to generate a profile that is equivalent to an optimal control based path. First, the ability to complete a desired maneuver in both axes at the same time is developed. This requires the ability to

adjust the length of the projected coast period in Bang-off-Bang maneuvers, based on independent axis maneuver times, to match a given profile. Effort was made to ensure that the code generated was as general as possible with the intention of having it be applicable to numerous situations.

1. Computation of Standard Maneuver Profile

For rest-to-rest motion between two given angles, the trapezoidal maneuver profile can be determined from Equation (5.1), after [17].

$$s(t)=\begin{cases}\dfrac{\omega\tau_1^2}{2T_1}; & 0<\tau_1\le T_1\\ \omega\tau_2+\dfrac{\omega T_1}{2}; & 0<\tau_2\le T_2\\ -\dfrac{\omega\tau_3^2}{2T_3}+\omega\tau_3+\theta-\dfrac{\omega T_3}{2}; & 0<\tau_3\le T_3\end{cases} \tag{5.1}$$

The segment from $0<\tau_1\le T_1$ describes the position of a gimbal through the acceleration phase. The $0<\tau_2\le T_2$ segment gives the position during the coast phase. The interval, $0<\tau_3\le T_3$, gives the position values during deceleration. Here, the values of position are represented by θ, rate is given by ω, and time parameters, T, are as described in Equations (5.2) and (5.3). Terms A and D represent the magnitude of the acceleration and deceleration, respectively.

$$T_1=\frac{\omega}{A};\quad T_3=-\frac{\omega}{D} \tag{5.2}$$

$$T_2=\frac{\theta}{\omega}-\frac{(T_1+T_3)}{2} \tag{5.3}$$

The summation of the times resulting from Equations (5.2) and (5.3), $T=T_1+T_2+T_3$, were used to calculate the total maneuver time. The associated rate and acceleration profiles can be calculated by taking the first and second derivatives of the position expression given in Equation (5.1). This results in the expressions given in Equation (5.4) for the three segments of the maneuver.

$$\begin{bmatrix} s_1(\tau) \\ v_1(\tau) \\ a_1(\tau) \end{bmatrix} = \begin{bmatrix} \frac{\omega\tau_1^2}{2T_1} \\ \frac{\omega\tau_1}{T_1} \\ A \end{bmatrix}; \qquad \begin{bmatrix} s_2(\tau) \\ v_2(\tau) \\ a_2(\tau) \end{bmatrix} = \begin{bmatrix} \omega\tau_2 + \frac{\omega T_1}{2} \\ \omega \\ 0 \end{bmatrix}; \qquad \begin{bmatrix} s_3(\tau) \\ v_3(\tau) \\ a_3(\tau) \end{bmatrix} = \begin{bmatrix} -\frac{\omega\tau_3^2}{2T_3} + \omega\tau_3 + \theta - \frac{\omega T_3}{2} \\ -\frac{\omega\tau_3}{T_3} + \omega \\ D \end{bmatrix} \quad (5.4)$$

The user must provide the desired maneuver distance $\left(\theta_f - \theta_o\right)$ and the system limits on acceleration, deceleration, and velocity. The MATLAB code generated for this simulation was based the pseudo-code contained in [17].

To ensure each axis completed its maneuver concurrently, the total time of all steps for each axis was evaluated. The velocity required for the axis with the lower total time was recalculated using the "vpasolve" numerical solver function in MATLAB. The trapezoid model was then run again for that axis with the resulting velocity limit. Note that in this approach the switch times may not be aligned in time.

2. Individual Axis Linear Motion Profile

In order to begin testing the basic equation for the path matching approach, a simple test was performed. A large maneuver was simulated using the generated model to validate the execution of Equation (5.4). This method also provides a base case for maneuver time in tests that follow. First, a linear maneuver of 10 degrees elevation and 80 degrees azimuth was generated from Equation (5.4). Acceleration and deceleration were limited to 0.045°/s^2 and velocity was limited to 0.225°/s. This results in the motion profiles shown in Figure 21.

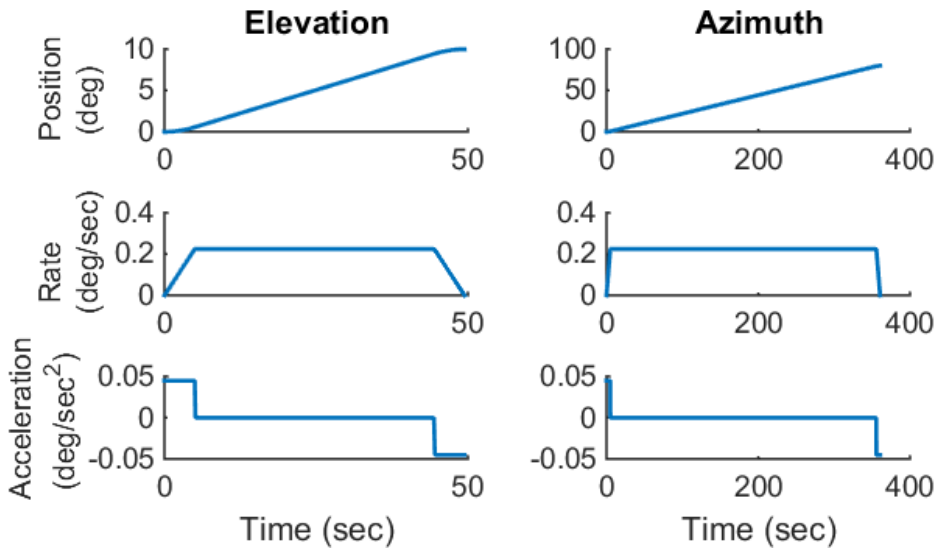

Figure 21. Asynchronous linear motion profile results for independent axes.

Here, the total maneuver times are 49.4 seconds for elevation and 360.5 seconds for azimuth. Note this maneuver uses the maximum allowable velocity for each axis resulting in the different slew times for each axis. The simulation was run again to verify the ability to match the final time of each maneuver with updated velocity values. The velocity calculation is fully automated as part of the maneuver generation script. The synchronous maneuver is shown in Figure 22.

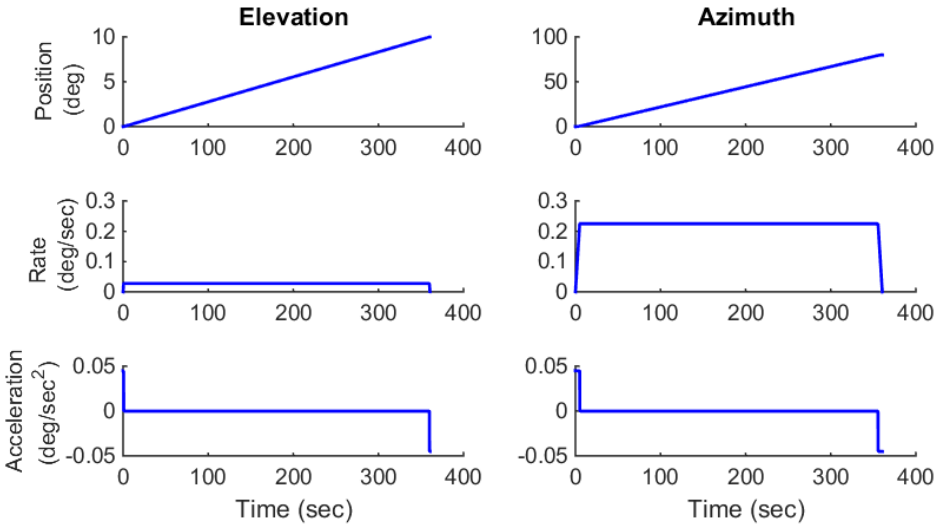

Figure 22. Synchronous linear motion profile for independent axes.

Note the final times for each axis of the synchronous maneuver coincide at 360.5 seconds. This is a result of decreasing the maximum value of elevation velocity to 0.028 °/s. The maximum value of acceleration is also used for both axes for varying amounts of time to reach the desired rate limit.

3. Stepped Motion Profiles

Applying Bellman's Principle, an optimal path can be divided into a sequence of maneuver steps which are each optimal, as long as the steps follow the original reference trajectory [18]. This is demonstrated in Figure 23, where an optimal path has been divided into five individual steps. Under certain conditions, as shown in Chapter III, the Bang-Bang and Bang-Off-Bang acceleration profiles represent the optimal control solution. So splitting the maneuver into a number of steps is consistent with Bellman's Principle. Optimal trajectories for more complicated systems can, in theory, be matched using a sequence of these rudimentary maneuvers. The definition of Bellman's Principle will not be satisfied exactly in this case. However, the idea is that a near optimal trajectory can be reproduced, in the spirit of Bellman, using a collection of near optimal steps.

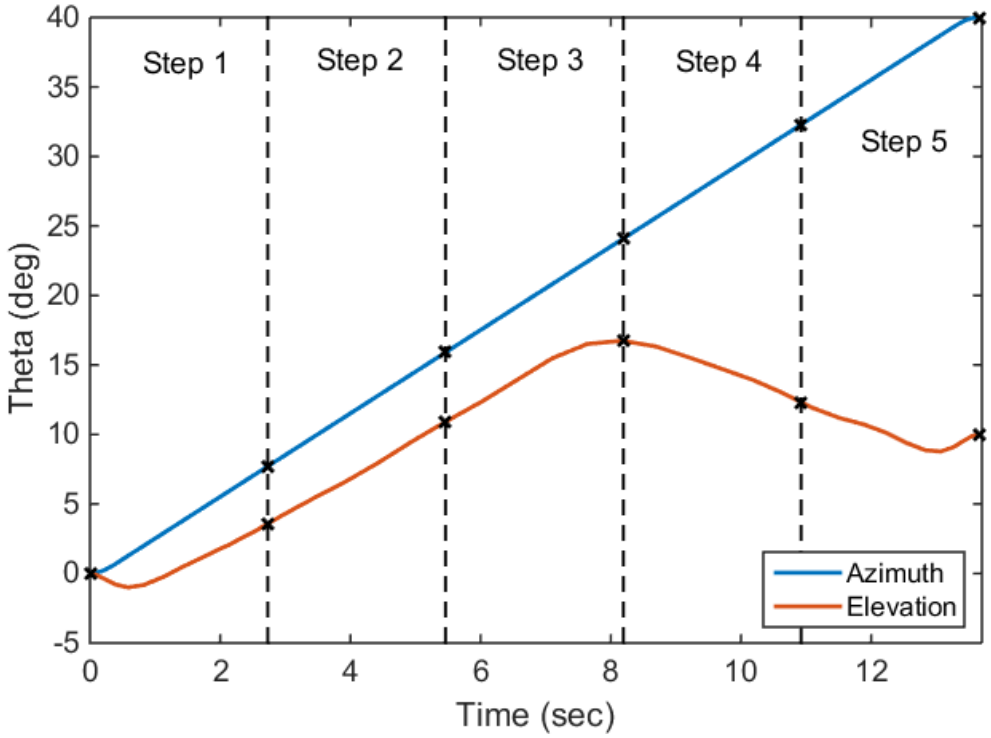

Figure 23. Division of an optimal motion profile into steps using Bellman's Principle.

To investigate this idea, the profile model described above was modified to incorporate the ability to perform rest-to-rest, uniform time steps, over a given time interval, to produce a desired path. Since each step requires the boundary conditions to be met before proceeding to the next one, the total time required for the matched profile must be compared to the optimal reference maneuver. A test case was run with five steps to verify that a standard maneuver profile could be produced and to evaluate the effects of additional steps on total maneuver time. The results are shown in Figure 24.

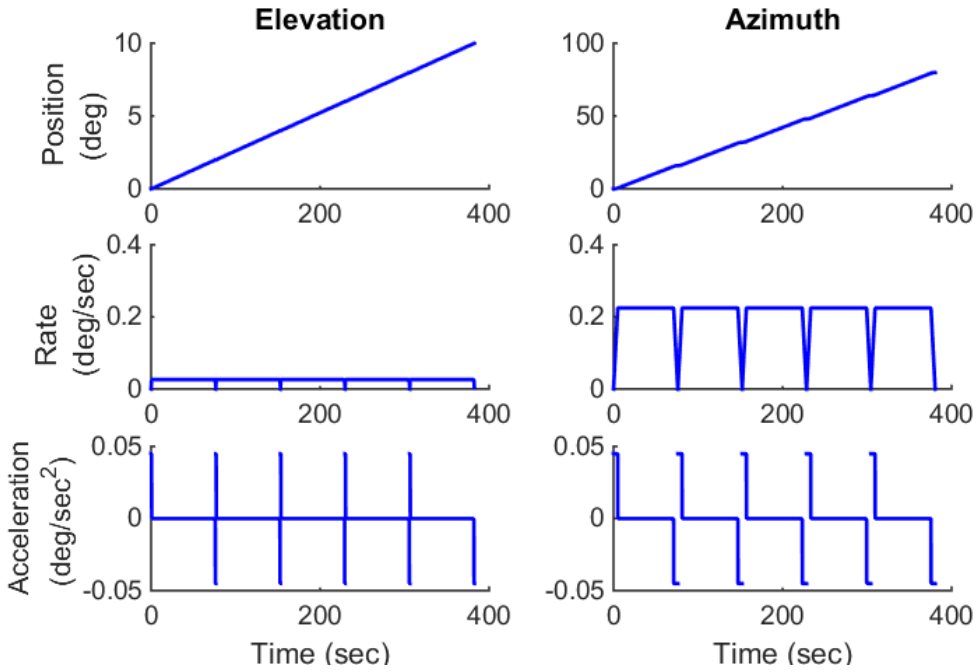

Figure 24. Multi-step linear motion profile for independent axes.

The results of Figure 24 display similar behavior to the case shown in Figure 22. The total maneuver time for the multi-step profile is 382.9 seconds, a full 22 seconds longer than the original case. This is a result of the individual steps being rest-to-rest: additional time is required to bring the rate of each axis to zero before moving on to the next step.

The amount of additional time required is related to the number of steps used to match the desired position profile. This is not a significant issue in this trivial case but becomes more of an issue as the motion profile becomes more complicated, since capitalizing on the effects of non-linear coupling terms depends on accurately reproducing each axis motion profile.

B. MOTION MATCHING TESTS

The trivial maneuver of the last section was used for development and troubleshooting of the trapezoid motion profile model. Generally, optimal control results are of a polynomial form and resemble more of an S-curve for the position variables. Therefore, two additional test cases were evaluated with this model to fully vet the

developed code: a sinusoidal profile and the results of the double gimbal optimization from Chapter IV.

1. Sinusoidal Motion Profile Generation

A sine function was used to develop a non-linear motion profile from the trapezoid motion model described in Section A. No reference path was used for these simulations, the desired motion profile was created directly using azimuth values from $0 \le Az \le 2\pi$, where $Az = 2\pi / N$ and N is the number of steps. Elevation angles are given by $El = \sin(Az)$. This test did not consider the maneuver time, only the desired motion path of the axes.

The range of azimuth angles was chosen to demonstrate positive and negative changes in elevation axis angles and to give a full cycle of the sine wave. Figure 25 presents the output of the trapezoid motion algorithm when the time was split into evenly spaced steps. For this test case, N = 10 was chosen arbitrarily to provide enough points to produce a relatively smooth sine wave.

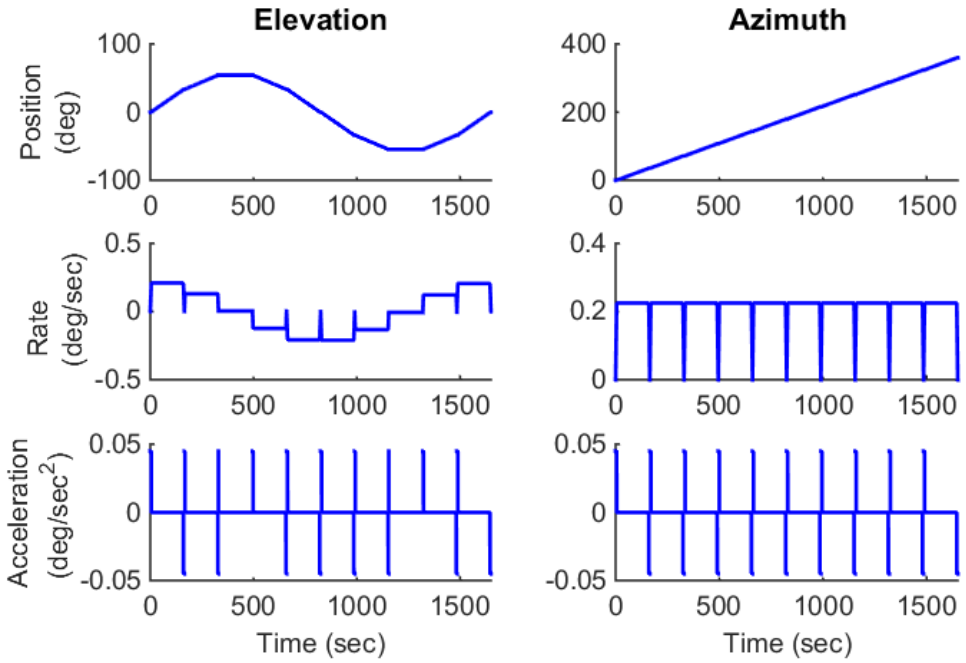

Figure 25. Multi-step sinusoidal motion profile for independent axes.

2. Double Gimbal Optimal Path Matching

While the cases presented previously are useful for proof of concept, they are contrived. The double gimbal system optimization described in Chapter IV was used next to test the developed path matching model, with an optimal result. For this test, the double gimbal was maneuvered in minimum time from 0° to 40° azimuth and 0° to 10° elevation. The maximum rate was limited to 3°/s for each axis. The optimal maneuver was then matched using a sequence of five rest-to-rest steps.

This is also the first test case to use data imported from a DIDO output file. This required slight modification of the code to include importing the .mat file and employing the interpolate tools to divide the optimal path into steps. Figure 26 shows the resulting five step approximation of the optimal path along with the DIDO result for each axis. Note that the curves labelled "Profile Match" are obtained using linear interpolation. Only the initial and final points of each segment (indicated by "x" markers) are used by the path matching algorithm.

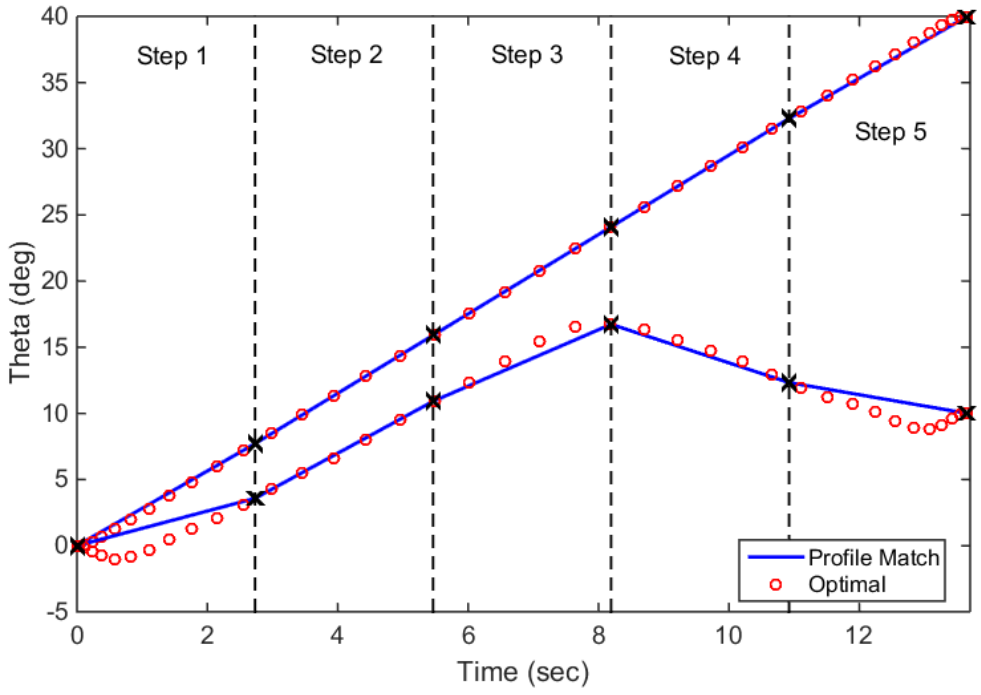

Figure 26. Division of optimal motion profile for minimum time double gimbal problem into steps.

In this example, the time optimal path reaches the desired final conditions in 13.65 seconds, based on the conditions described. Solving a maneuver for each axis independently using the method described in Section A.2 gives a maneuver that is 14.33 seconds long. This optimal path represents a 4.7% improvement in maneuver time. Evidently, coupling effects allow the maneuver to be completed more quickly.

While this particular result varies in many respects from the case presented in Chapter IV.B.1, the general shape of each axis motion path is preserved. This is the first example of an optimal path that takes advantage of dynamic coupling among the various bodies of the system to reduce the maneuver time. This result, therefore, presents a more realistic case for analysis and is closer to the real world systems for which this thesis is intended to be of benefit. Five steps were chosen to ensure reasonable approximation of the optimal solution but no quantitative analysis of fit quality or step sensitivity was performed. The results of the simulation output are provided in Figure 27.

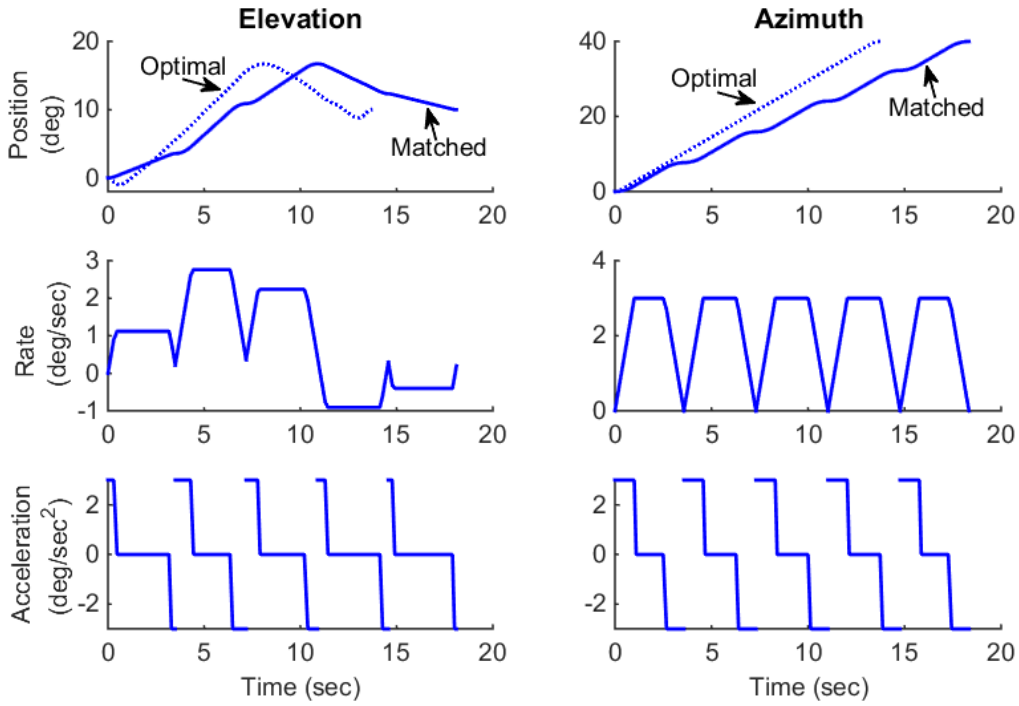

Figure 27. Multi-step optimal motion profile for time optimal double gimbal problem (rest-to-rest steps).

This model performs reasonably well in matching the shape of the input provided but requires 18.33 seconds to complete the maneuver. This is a 27.9% reduction in performance over the current state of practice and is 34.3% worse than the optimal path. It is also unlikely that any coupling benefit would be retained by this matched maneuver. While the situation could be improved by varying the number of steps, the main reason for this additional time requirement is the rest-to-rest nature of each step in the process.

C. IMPROVING PERFORMANCE ON VARIABLE MOTION PROFILES

The results of the rest-to-rest test cases demonstrated the concept of optimal path matching is feasible but cause the maneuvers to take longer to complete. One approach for improving model performance is to allow for non-zero initial and final velocity values in the intermediate steps of the maneuver path so that both position and velocity can be matched. This was accomplished using a MATLAB script previously developed by Karpenko, available from the author [19].

This function replaced the rest-to-rest motion generator. The new function takes reference values for both gimbal axes positon and rate into account during calculation. Now the input provided includes the segment's initial and final position and velocity, the step time, and the acceleration and deceleration limits. Because the step time is specified, total generated maneuver time should match the optimal path provided. The function tests maneuver feasibility based on the provided limits, and then produces a trajectory that works to maintain the rate and position profile of each axis concurrently.

To test the potential for this refined approach, the results from the minimum time double gimbal case were re-evaluated. As in the other initial test cases five steps were chosen. The results for position, velocity, and acceleration obtained for each axis are presented in Figure 28. The simulation results now closely match the optimal reference profile. The final time for each is 13.65 seconds, which is consistent with the optimal solution. As can be seen, the velocity and position trajectories are not exactly matched. This suggests that additional steps are needed. Another case was run with ten steps and the results are shown in Figure 29. Evidently, including additional steps reduces the matching error.

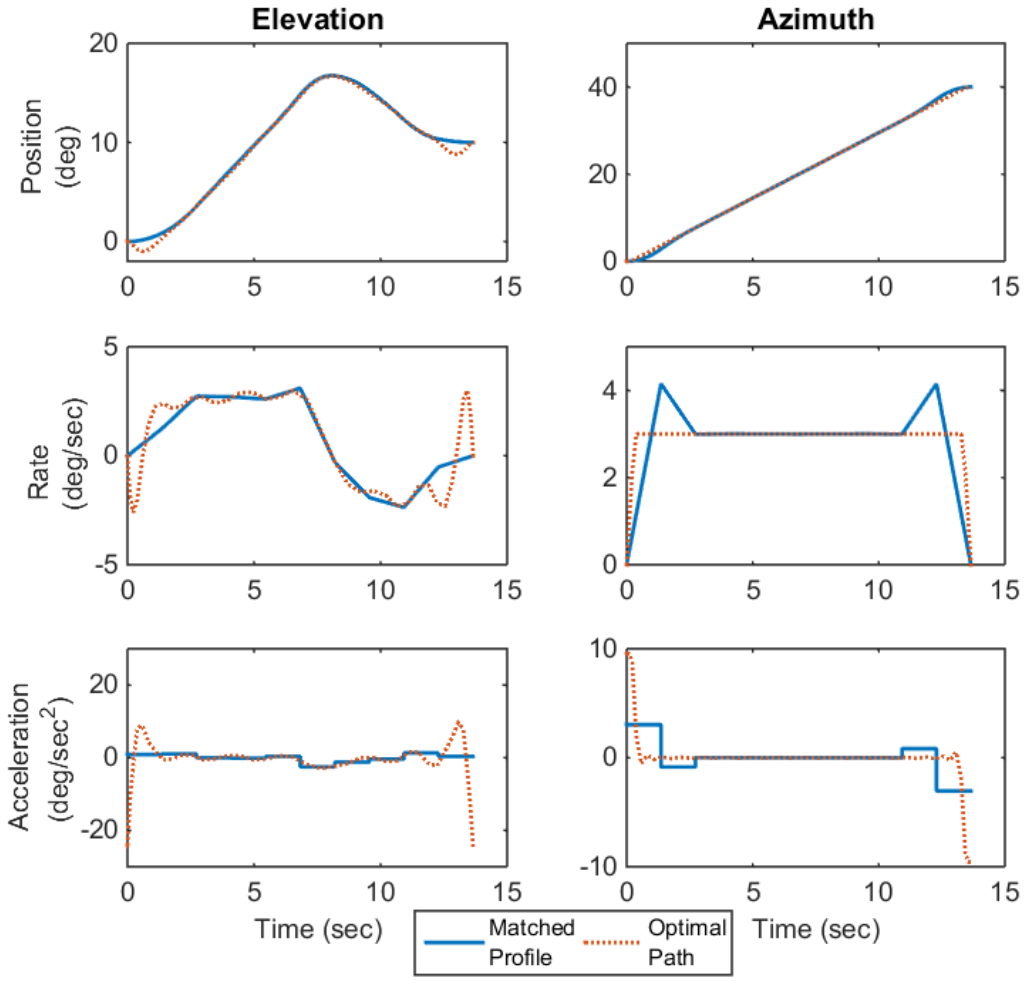

Figure 28. Multi-step optimal motion for time optimal double gimbal problem (5 non-rest steps).

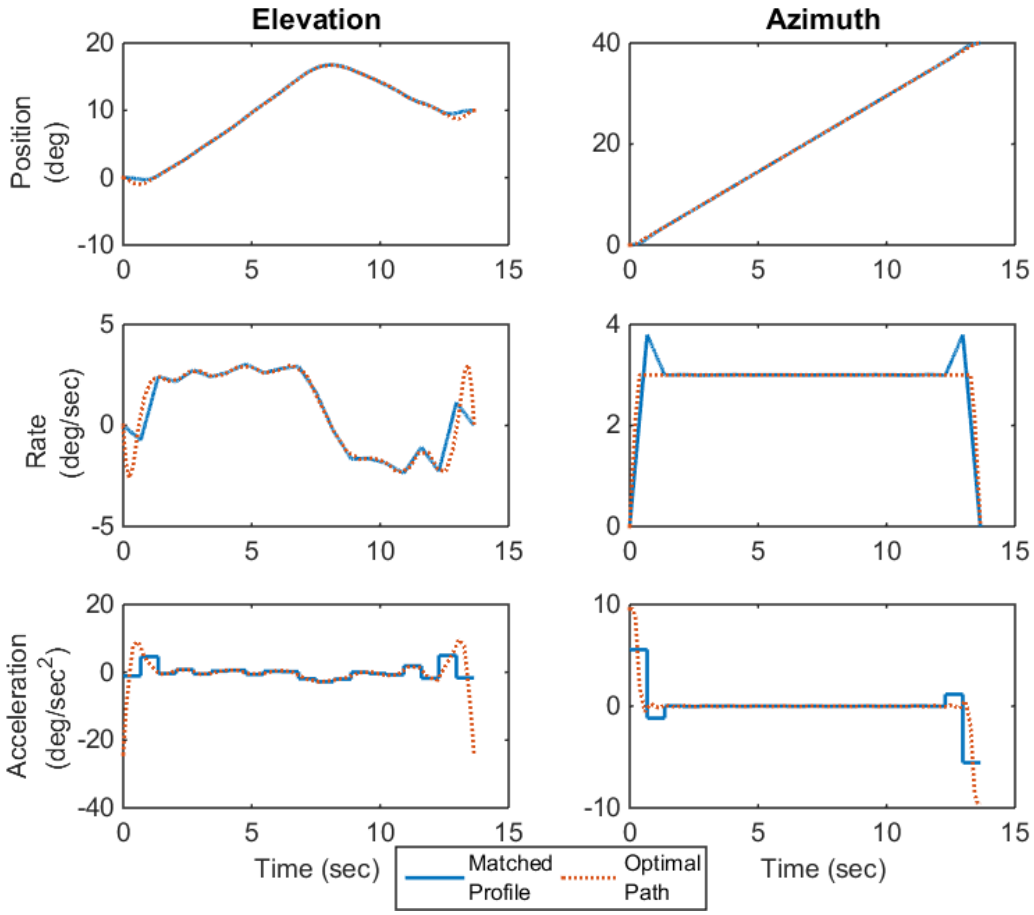

Figure 29. Multi-step optimal motion for time optimal double gimbal problem (10 non-rest steps).

These results of Figures 28 and 29 lead to the question of how many steps need to be used to generate the desired rate and position profiles. Applying too few steps will reduce accuracy, while applying additional steps may not significantly improve accuracy leading to unnecessary complexity. The ideal number of steps must be determined in order to meet user requirements. To determine the best number of steps to use the matching quality of the generated profile against the optimal reference profile can be evaluated. The 1-norm and 2-norm of the maneuver path length are suitable metrics for this purpose.

The 1-norm is defined by [20];

$$\|x\|_1 = \sum_{i=1}^{m} |x_i| \tag{5.5}$$

while 2-norm is defined by [20] ;

$$\|x\|_2 = \left(\sum_{i=1}^{m} |x_i|^2 \right)^{1/2} \tag{5.6}$$

and the reproduction error can be calculated as:

$$Fit\ Error = \frac{\|(Matched - Reference)\|}{\|Reference\|} \tag{5.7}$$

All norm values were calculated using MATLAB's norm function. The 1-norm verifies the sum of each path vector generated by the simulation is the same as the reference path. The 2-norm determines the Euclidean length of each path vector [20]. These values are then compared to the reference to determine a matching error quality. A perfect match would yield a zero result using Equation (5.7).

These measures of error were chosen because they provide a comparison of the entire generated path to the reference trajectory. An alternative method would measure the error for each step to determine how closely reference path points were matched. This would be appropriate if the matching code was based on executing the desired control profile over the step time interval and measuring the performance versus the optimal reference path. This method was not chosen because the matching code developed requires the system to reach the desired end point for each step before switching to the next target point. The measures described in Equations (5.5)–(5.7) will be used in the remainder of the thesis to determine the reference path matching quality of simulation result.

The error metrics are now used to perform a step sensitivity analysis. An iterative loop was developed in MATLAB to determine the error of results for a range of step values from one to a user defined maximum (in this case five). The optimal reference

path was matched using the allowed number of steps and the error metrics computed. The results were compared to the reference using Equation (5.7) producing Figure 30, which presents the results for the minimum time double gimbal maneuver discussed in this section.

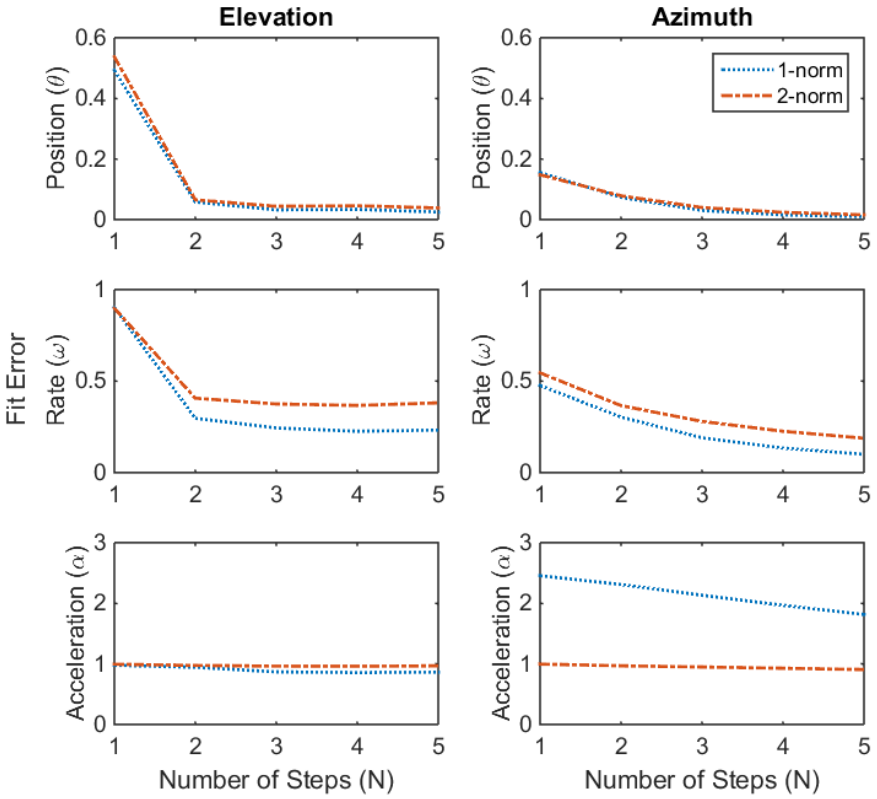

Figure 30. Fit error sensitivity for the minimum effort double gimbal problem.

In Figure 30, the position matching performance appears to converge at three steps for azimuth and two steps for elevation. These results follow the qualitative error trends observed in Figure 28. For this test case, the maximum number of steps allowed was increased to ten with no significant reduction in calculated rate or position error after five steps. This error analysis also shows that five steps (as in Figure 28) provide a good match of the desired, optimal reference trajectory.

The error analysis allows the user to select a sequence of steps that meet the error tolerance desired for the application in question. Using too few steps may reduce the

efficiency of the maneuver to a point that the benefit does not justify the changes necessary to implement this method. Using too many steps, on the other hand, unnecessarily complicates the process.

D. SUMMARY

This chapter demonstrates that an optimal reference trajectory can be reproduced using a series of Bang-Bang and Bang-Off-Bang steps. Requiring rest-to-rest behavior for these steps increased the total maneuver time, but employing non-rest intermediate steps allowed the optimal reference profiles to be more closely reproduced. A simple error analysis was developed to help determine the correct number of steps necessary to accurately reproduce the desired profile. These results are promising but are based on simplified example cases. Next, the developed approach will be employed on the real world TDRS antenna slew problem.

VI. APPLICATION TO TDRS

Chapter V demonstrated that various optimal trajectories can be implemented with current kinematics based control techniques for a simple, theoretical system. In this chapter, the same approach is applied to a real world system to evaluate the utility of this method for a practical problem. Specifically, the work of Sears [1], on optimizing the antenna slews of NASA's TDRS satellite, was used as a test case. TDRS uses two single-access (SA) antennas, shown in the schematic of Figure 31, to support the bulk of its communication services.

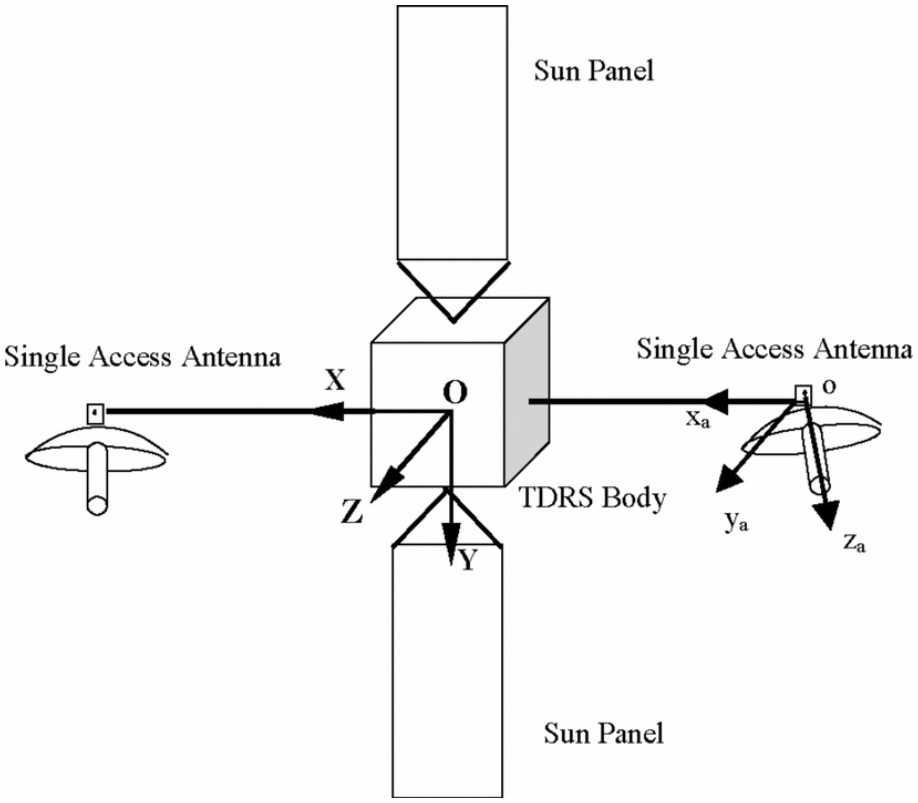

Figure 31. Simplified schematic of TDRS, from [21].

TDRS provides a link to ground stations for tracking and data relay services for satellites in altitudes ranging from 750 to about 3,100 miles [21]. An overview of the opportunity for slew improvement, development of a system dynamic model, and its optimization as presented in [1] will be discussed in this chapter. Results from applying

the techniques of Chapter V to optimized TDRS antenna slews will also be presented to show how optimal antenna slew profiles could be implemented on this legacy system.

A. TDRS MODEL

The TDRS system (TDRSS) presents an opportunity to improve customer access to a satellite relay by improving the efficiency of its antenna slews. Currently, TDRSS antenna slew maneuvers are planned to occur over a standard three minute window [1]. In the event that a maneuver is calculated to take less time a buffer is added to extend the maneuver out to three minutes. Maneuvers that exceed the standard length, such as large slews from the limits of the antenna field of view, are planned for their full duration to provide customers accurate access time estimates [1]. These planning limitations can lead to reduced system employment and in some cases even excluded users, particularly during periods of congestion.

One of the drivers for the use of the three minute slew time for access scheduling is the current method of slew control used by TDRSS. A maneuver from one target to another requires three phases: a program track that performs the gross antenna slew, an acquisition phase to align the boresight toward the null, and a target lock phase where target tracking occurs [22]. Little effort has been applied to improve the gross antenna slew portion of these antenna maneuvers, with the work of [1], [21] being the notable exceptions.

The standard slew mode is designed to include three segments in a Bang-Off-Bang arrangement: 5 seconds of acceleration, constant rate coast to a pointing error less than 1.17 degrees, and a 5 second deceleration [21]. Each slew axis maneuver is determined independently. During the slew phase for large SA maneuvers ($>5^{o}$ in one gimbal axis), gimbal rate is limited to 0.25^{o}/s to reduce base motion effects in the satellite body and the coupled effects on the second SA antenna [6], [16]. This limit further reduces the performance of the slew phase in an effort to simplify control of the base body. In the case that one axis requires a larger slew than the other; the coasting phase slew rate is adjusted to ensure that both maneuvers are completed at the same time [1], [16].

Based on available literature, the dynamic model of TDRS used in the slew optimization problem described in [1] was developed. This model was derived based on the method presented in [14] for multi-body dynamic systems. The resulting equations were validated using MATLAB and SimMechanics. This analysis established the limits used in test cases for control torque and maximum spacecraft body rates [1].

An intermediate, expanded form of the equations of motion, developed following the method in [14], is given in Equation (6.1) [6].

$$\left[\begin{array}{cccc|cc} I_0 & 0 & 0 & 0 & -\tilde{r}_{01} & 0 \\ I_1 & I_1\Gamma_1 & 0 & 0 & \tilde{r}_{11} & -\tilde{r}_{12} \\ I_2 & I_2\Gamma_1 & I_2\Gamma_2 & 0 & 0 & \tilde{r}_{22} \\ 0 & 0 & 0 & m_0 & 1 & 0 \\ \hline m_1\left(\tilde{r}_{11}-\tilde{r}_{01}\right) & m_1\tilde{r}_{11}\Gamma_1 & 0 & m_1 & 1 & -1 \\ m_2\left(\tilde{r}_{11}-\tilde{r}_{01}+\tilde{r}_{22}-\tilde{r}_{12}\right) & m_2\left(\tilde{r}_{11}+\tilde{r}_{22}-\tilde{r}_{12}\right)\Gamma_1 & m_2\tilde{r}_{22}\Gamma_2 & m_2 & 0 & 1 \end{array}\right]\left[\begin{array}{c} \dot{\omega}_0 \\ \ddot{\theta}_1 \\ \ddot{\theta}_2 \\ \dot{\upsilon}_0 \\ \hline F_{G1} \\ F_{G2} \end{array}\right] = \left[\begin{array}{c} T_0 + T_{G1} - \tilde{\omega}_0 I_0 \omega_0 \\ T_1 - T_{G1} + T_{G2} - \tilde{\omega}_1 I_1 \omega_1 - I_1\dot{\Gamma}_1\dot{\theta}_1 \\ T_2 - T_{G2} - \tilde{\omega}_2 I_2 \omega_2 + I_2\left(\dot{\Gamma}_1\dot{\theta}_1 + \dot{\Gamma}_2\dot{\theta}_2\right) \\ F_0 \\ \hline F_1 - m_1\tilde{r}_{11}\dot{\Gamma}_1\dot{\theta}_1 + m_1\bar{\omega}_0 r_{01} - m_1\bar{\omega}_1 r_{11} \\ F_2 + m_2\left(-\tilde{r}_{11}+\tilde{r}_{12}-\tilde{r}_{22}\right)\dot{\Gamma}_1\dot{\theta}_1 - m_2\tilde{r}_{22}\dot{\Gamma}_2\dot{\theta}_2 + m_2\left(\bar{\omega}_0 r_{01} - \bar{\omega}_1 r_{11} + \bar{\omega}_1 r_{12} - \bar{\omega}_2 r_{22}\right) \end{array}\right] \tag{6.1}$$

Equation (6.1) and the results of multi-body simulations were used to formulate the optimal antenna slew problem. The basic optimal control problem statement with associated state and control limits is presented in Equation (6.2) [1]. The optimal control problem was solved using DIDO.

$$x = \left\{ \omega_0 \quad \dot{\theta}_1 \quad \dot{\theta}_2 \quad \theta_1 \quad \theta_2 \right\} \qquad u = \left\{ T_{G1} \quad T_{G2} \right\}$$

$$\textit{Minimize} \qquad J = \alpha t_f + \beta \int_{t_0}^{t_f} (\mathrm{T_{G1}}^2 + \mathrm{T_{G2}}^2) dt$$

Subject to:

$$\dot{\omega}_0 = \left[(A - RU^{-1}S)^{-1} (T' - RU^{-1}F') \right]_1$$

$$\ddot{\theta}_1 = \left[(A - RU^{-1}S)^{-1} (T' - RU^{-1}F') \right]_2$$

$$\ddot{\theta}_2 = \left[(A - RU^{-1}S)^{-1} (T' - RU^{-1}F') \right]_3$$

$$\left(\omega_0(t_0), \dot{\theta}_1(t_0), \dot{\theta}_2(t_0), \theta_1(t_0), \theta_2(t_0) \right) = \left([0,0,0], \dot{A}z_0, \dot{E}l_0, Az_0, El_0 \right)$$

$$(\dot{\theta}_1(t_f), \dot{\theta}_2(t_f), \theta_1(t_f), \theta_2(t_f)) = (\dot{A}z_f, \dot{E}l_f, Az_f, El_f)$$

$$\begin{aligned}
-1 \le \dot{\theta}_1(t) \le 1 \quad & \text{deg/ } s \\
-1 \le \dot{\theta}_2(t) \le 1 \quad & \text{deg/ } s \\
-72 \le \theta_1(t) \le 24 \quad & \text{deg} \\
-32 \le \theta_2(t) \le 32 \quad & \text{deg} \\
-0.0022 \le \omega_{0,x}(t) \le 0.0022 \quad & \text{deg/ } s \\
-0.025 \le \omega_{0,y}(t) \le 0.025 \quad & \text{deg/ } s \\
-0.0126 \le \omega_{0,z}(t) \le 0.0126 \quad & \text{deg/ } s \\
0.2 \le T_{G1}(t) \le 0.2 \quad & N \cdot m \\
0.2 \le T_{G2}(t) \le 0.2 \quad & N \cdot m
\end{aligned} \tag{6.2}$$

B. TEST CASES

In order to use DIDO for slew path optimization, initial and final maneuver conditions including azimuth, elevation and their associated rates must be determined. For the cases presented in [1], simulations were performed using Systems Tool Kit (STK) software, a powerful orbit propagator capable of generating azimuth and elevation data. Four customer spacecraft representing various target positions and TDRS were placed in an orbital model that was propagated for a 24-hour period [1]. Customer spacecraft involved in the simulation include: the International Space Station (ISS), National Oceanic and Atmospheric Administration (NOAA) 15, Worldview 2, and a fictional MEO satellite. The orbital parameters used for these satellites are summarized in Table 4.

Table 4. Target satellite orbital elements, from [1].

	TDRS	ISS	NOAA-15	Worldview-2	MEO
Semi-Major Axis (km)	42166.41	6787.36	7173.81	7150.06	16678.14
Eccentricity	0.001014	0.001563	0.002720	0.001403	0.500000
Inclination (deg)	2.730	51.595	98.708	98.504	20.000
[1]RAAN (deg)	64.113	330.089	330.583	58.213	0
[2]Arg of Perigee (deg)	187.147	98.819	65.831	74.292	360
[1]Right Ascension of Ascending Node					
[2]Argument of Perigee					

A sixth satellite in a geostationary orbit 72^{o} outboard in azimuth, in the same inclination and at the same ascending node as TDRS was added to investigate the effects of the full antenna FOV [1]. This satellite was not included in the simulation because its position and rate relative to TDRS were known. The output of the STK simulation and the known information about the sixth satellite identified six different scenarios where TDRS was required to slew from one customer to another. Azimuth and elevation angles and rates were calculated as boundary conditions for optimal control. These values for each scenario, as well as which customers are involved, are presented in Table 5.

Table 5. Boundary conditions for slew optimization, from [1].

	Scenario 1	Scenario 2	Scenario 3	Scenario 4	Scenario 5	Scenario 6
Starting Azimuth (deg)	-5.67	-9.07	7.52	-29.42	-8.84	-72.00
Starting Azimuth rate (deg/s)	-0.0006	0.0065	-0.0070	0.0002	0.0017	0.0000
Ending Azimuth (deg)	-8.27	-3.83	8.24	5.19	-24.19	8.24
Ending Azimuth rate (deg/s)	0.0054	-0.0063	-0.0053	0.0035	-0.0007	-0.0053
Starting Elevation (deg)	-7.35	-2.05	6.12	-7.21	-0.86	0.00
Starting Elevation rate (deg/s)	0.0005	0.0030	0.0071	-0.0010	-0.0077	0.0000
Ending Elevation (deg)	-5.16	8.92	5.16	6.97	1.42	5.16
Ending Elevation rate (deg/s)	-0.0086	-0.0038	0.0085	0.0011	-0.0012	0.0085
Scenario 1: ISS to NOAA-15						
Scenario 2: MEO to Worldview-2						
Scenario 3: NOAA-15 to Worldview-2						
Scenario 4: MEO to ISS						
Scenario 5: ISS to MEO						
Scenario 6: GEO to Worldview-2 (Same final conditions as Scenario 3)						

Optimal maneuver results for the scenarios using the limits on gimbal rate listed in Equation (6.2) yielded negligible benefit [1]. In order to achieve beneficial improvement in slew times, the gimbal rate limits were allowed to reach up to 2^{o}/s to provide a wide solution space. The gimbal rate limit was assumed to be a soft limit aimed at reducing the effects of SA gimbal slews on the spacecraft body and the second SA antenna and not a hard limit of gimbal hardware [1], [6]. However, in order to prevent the antenna motion from perturbing the spacecraft, limits on the induced spacecraft rates were imposed. Each scenario was optimized twice; the first run determined the minimum time solution and a second was used to minimize the control effort keeping the upper time bound the same as the value determined in the minimum time solution. This produced spacecraft body rotation results which all remained within acceptable limits while reducing slew times [1]. Table 6 presents a summary of results for each scenario including the estimated conventional maneuver time, optimal slew time obtained from DIDO and the percent reduction in time obtained.

Table 6. Optimal antenna slew results, from [1].

	Scenario 1	Scenario 2	Scenario 3	Scenario 4	Scenario 5	Scenario 6
Estimated Conventoinal Time (s)	17.13	54.32	9.80	159.40	73.78	362.17
Optimal Slew time (s)	16.44	40.12	8.66	87.56	56.03	122.60
Maximum Azimuth rate (deg/s)	0.2347	0.2351	0.1576	0.4688	0.4053	1.0214
Maximum Elevation rate (deg/s)	0.1806	0.3294	0.2051	0.2786	0.0617	0.0776
% reduction in slew time	4.03	26.14	11.62	45.07	24.05	66.15

In general, the largest reductions were seen where larger maneuvers are required. The increased gimbal slew rates allow the longer axis to build rate to decrease the slew time while the shorter maneuver axis slews in a non-traditional manner to help reduce the impact of the induced motion on the spacecraft body. The maneuvers of the larger axis follow a Bang-Bang type control profile accelerating through half the slew and decelerating for the other half. The smaller axis changes constantly to maintain the desired spacecraft body spins rates within their limits [1].

Implementation of the optimal path requires the use of the developed polynomial paths as reference profiles. Current methods to incorporate this type of path require

processing capabilities and software changes for existing systems. Thus, the optimal matching methods discussed in Chapter V present a less complicated and less costly alternative for realizing the benefits of the optimal solutions.

C. MATCHING OPTIMAL PATHS FOR TDRS ANTENNA SLEWS

The methods presented in Chapter V were applied to the results obtained from [1] to show how the optimal maneuvers can be implemented on a real-world system.

1. Scenario One

Scenario one was chosen as the first case to evaluate the performance of optimal maneuver matching. This scenario demonstrates the performance of TDRS on a routine, short maneuver and is presented as proof of concept for a real world application. The number of steps providing efficient matching was evaluated first and results for azimuth and elevation are presented in Figure 32.

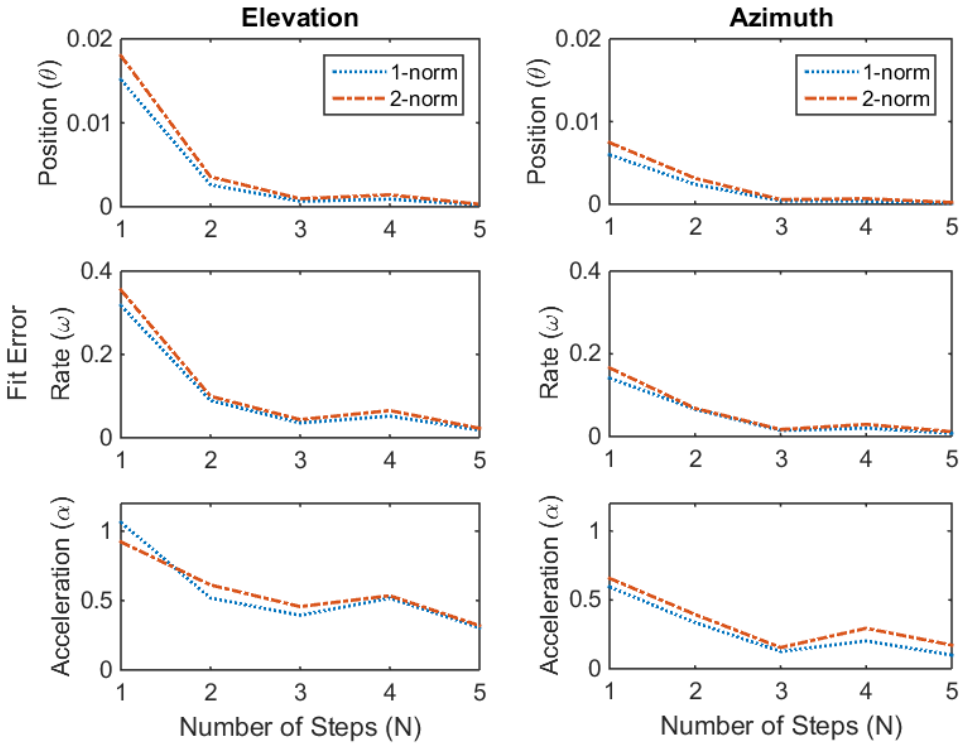

Figure 32. Fit error sensitivity of elevation and azimuth for Scenario one.

From the data shown in Figure 32, $N = 3$ was chosen as the number of steps to be used for further analysis and optimal maneuver matching. Figure 33 presents the $N = 3$ matched path (solid line) along with the optimal path (circles). Note that the error decreases from acceleration to rate to position as would be expected based on the integral relationship between these states. The final time of the matched profile is the same as the optimal reference path, 16.44 seconds. Finally, the quality of the matching path was compared to the values of the optimal path. For this scenario, the position follows to <0.1% error for both axes. Figure 34 presents the resulting error norms values for this case.

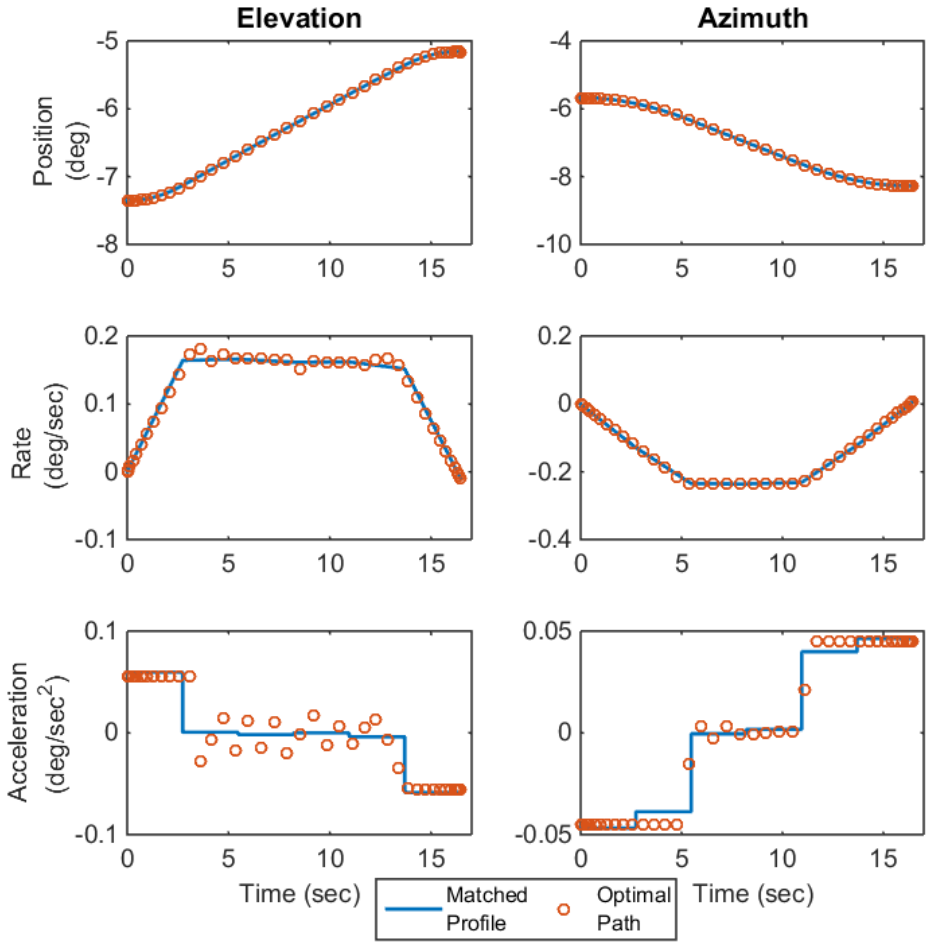

Figure 33. Matched profile with optimal path for scenario one with $N = 3$.

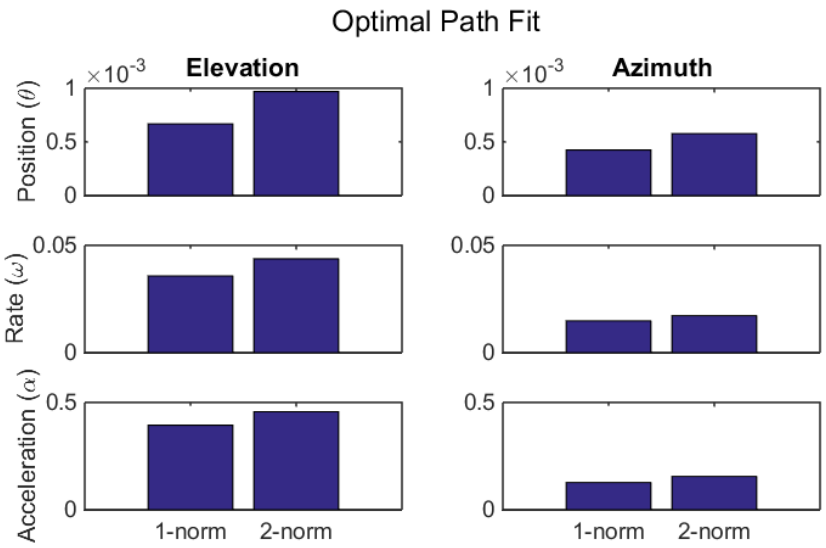

Figure 34. Fit error of elevation and azimuth for scenario one with $N = 3$.

2. Scenario Three

Scenario three was chosen for analysis based on the observation that both axes demonstrated close to a Bang-Bang behavior. This case verifies the proper behavior of the matching method by demonstrating a one-step match for this very short maneuver case (around 1^{o} in each axis). Azimuth and Elevation step sensitivity results are presented in Figure 35. Step sensitivity analysis shows that while there is some improvement when using more than one step, results are better at one step in this case than those for three or more steps in scenario one. This is likely because the maneuvers in each axis are short and the maximum acceleration is not reached in either axis. Figure 36 presents the matched path along with the optimal trajectory. Note that the error behavior is similar to scenario one.

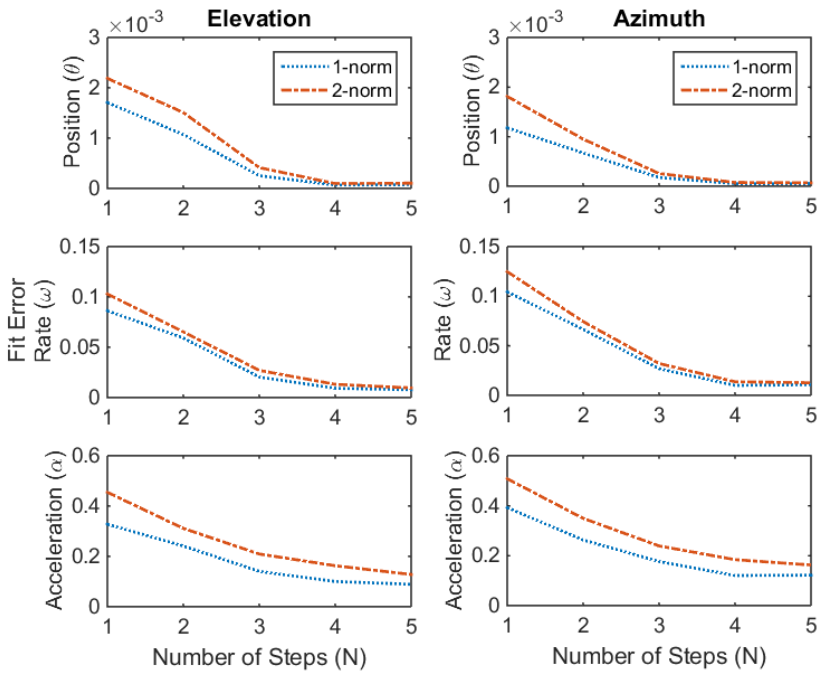

Figure 35. Fit error sensitivity of elevation and azimuth for scenario three.

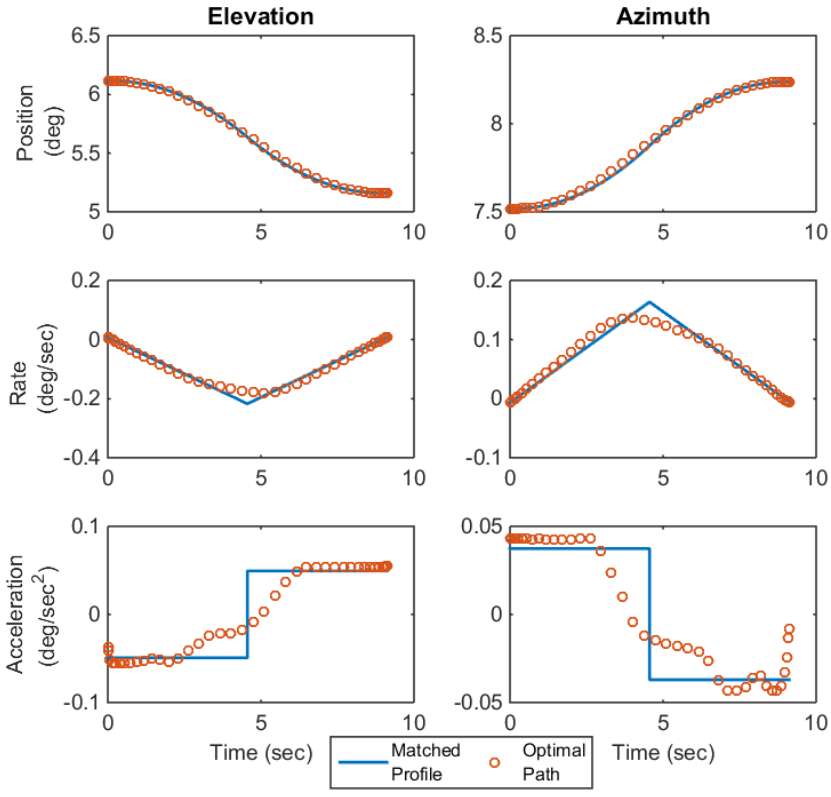

Figure 36. Matched profile with optimal path for scenario three with $N = 1$.

Finally, the quality of the matching path was compared to the values of the optimal path. For this scenario, the position follows to <0.3% error of the optimal path for both axes. Figure 37 presents the resulting error norm values for this case.

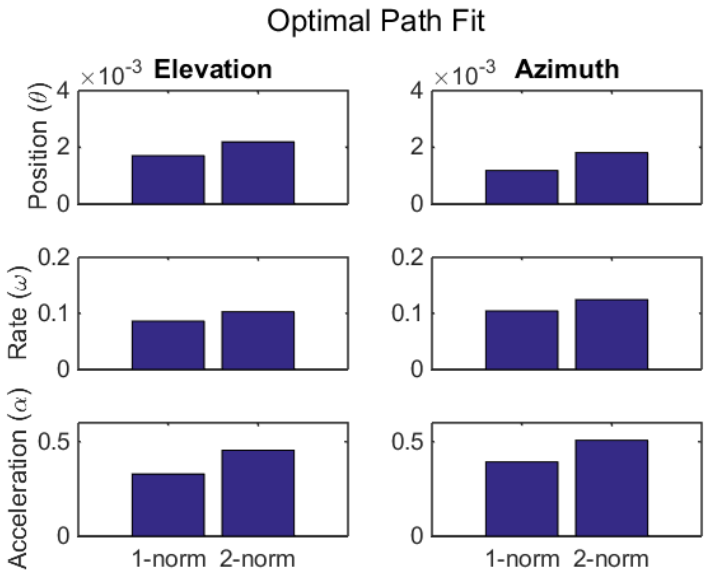

Figure 37. Fit error values of elevation and azimuth for scenario three with $N = 1$.

3. Scenario Six

Scenario six was the final case chosen for testing the maneuver matching scheme because it represents the largest maneuver analyzed and the largest improvement as noted in Table 6. For this case, the effects of varying number of steps were investigated. The simulation step sensitivity analysis for each axis is presented in Figure 38.

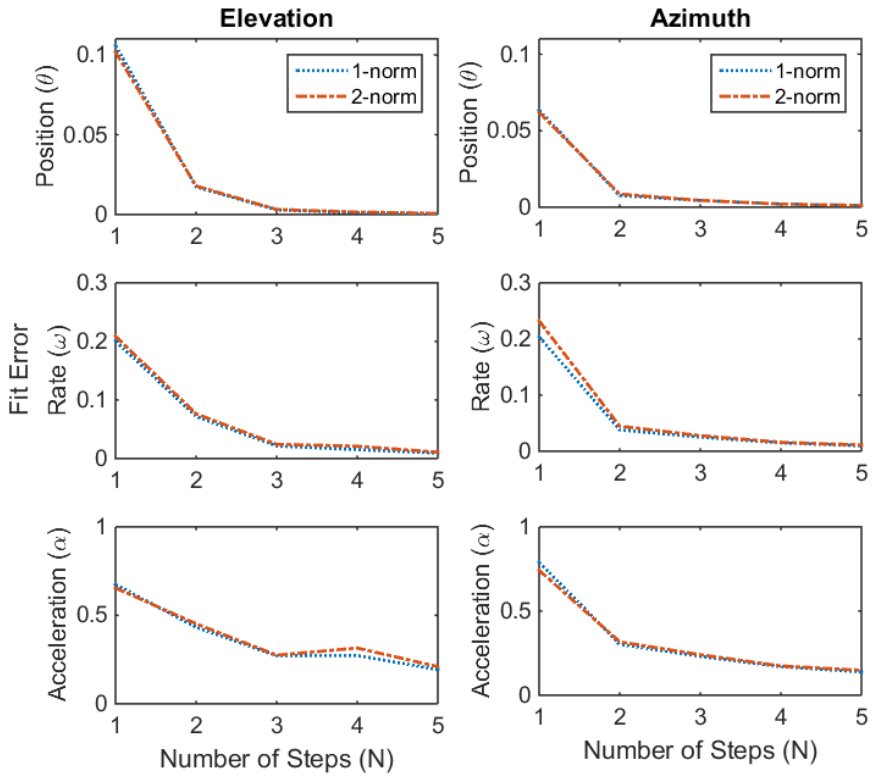

Figure 38. Fit error sensitivity of elevation and azimuth for scenario six.

In this scenario, the error of the Azimuth (dominant) slew appears to have a nearly linear relationship with number of steps beyond $N = 2$. To investigate the effects of number of steps, the match was performed using $N = 2$, 3, and 4. Graphs of each match compared to the optimal path will be provided to demonstrate the effects of the step size on the quality of the match. The graphs of simulation results along with the optimal path for $N = 2$ are presented in Figure 39.

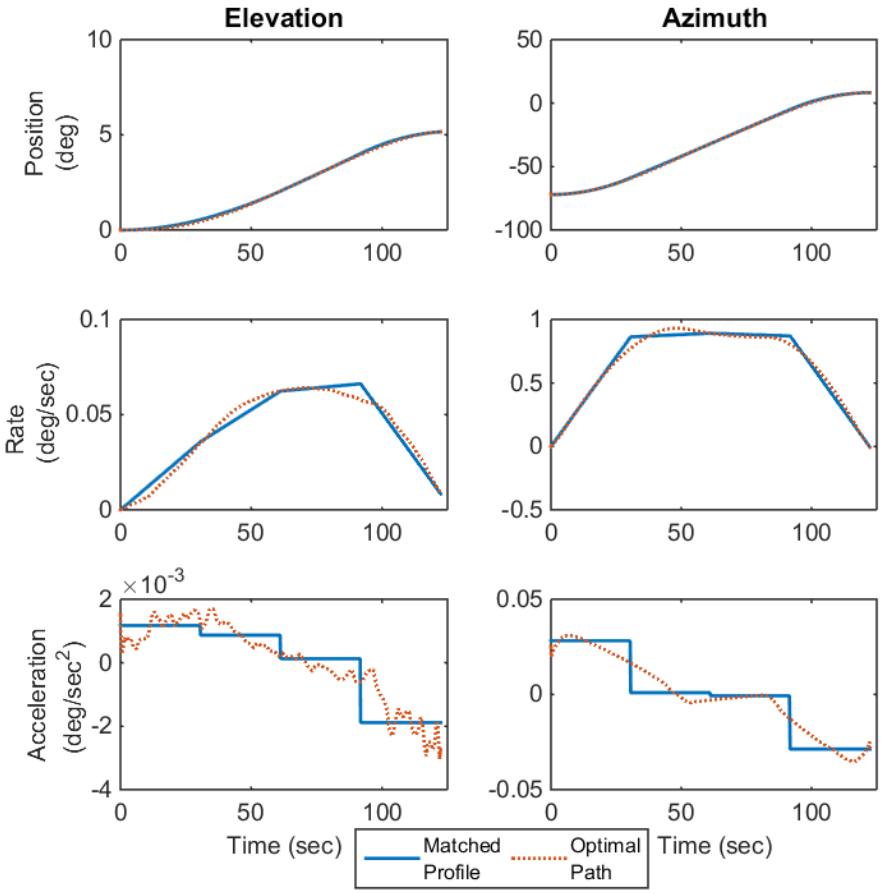

Figure 39. Matched profile with optimal path for scenario six with $N = 2$.

These results follow the same error behavior demonstrated in other cases analyzed. The final time of the matched path is the same as the optimal trajectory, 122 seconds. The quality of the matching path was compared to the values of the optimal path. For this scenario, the position error metric is less than 2% for both axes. Figure 40 presents the resulting fit error values for this case.

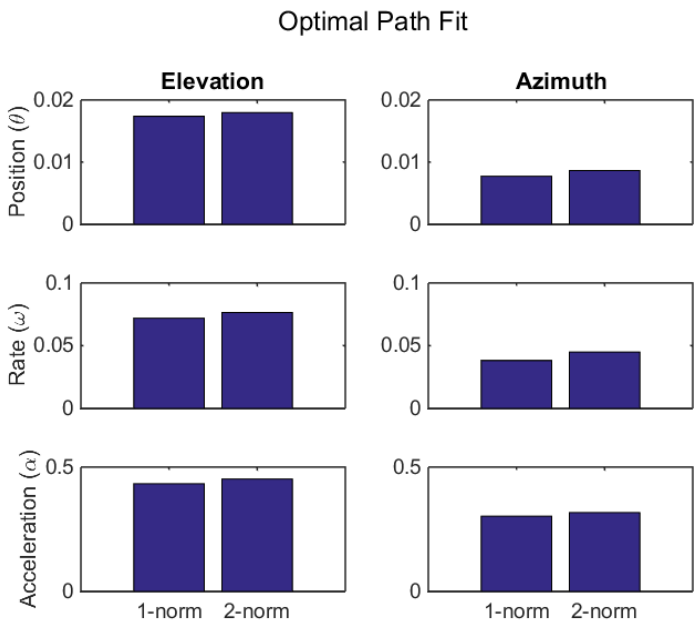

Figure 40. Fit error values of elevation and azimuth for scenario six with $N = 2$.

The graphs of simulation results with the optimal path for $N = 3$ are presented in Figure 41. Note the visual improvement in rate and position matching. For this scenario, the position error has been reduced to less than 0.5% for both axes. Figure 42 presents the resulting error norm values for this case, which confirm the perceived improvement in the maneuver trajectory as compared to the case where $N = 2$.

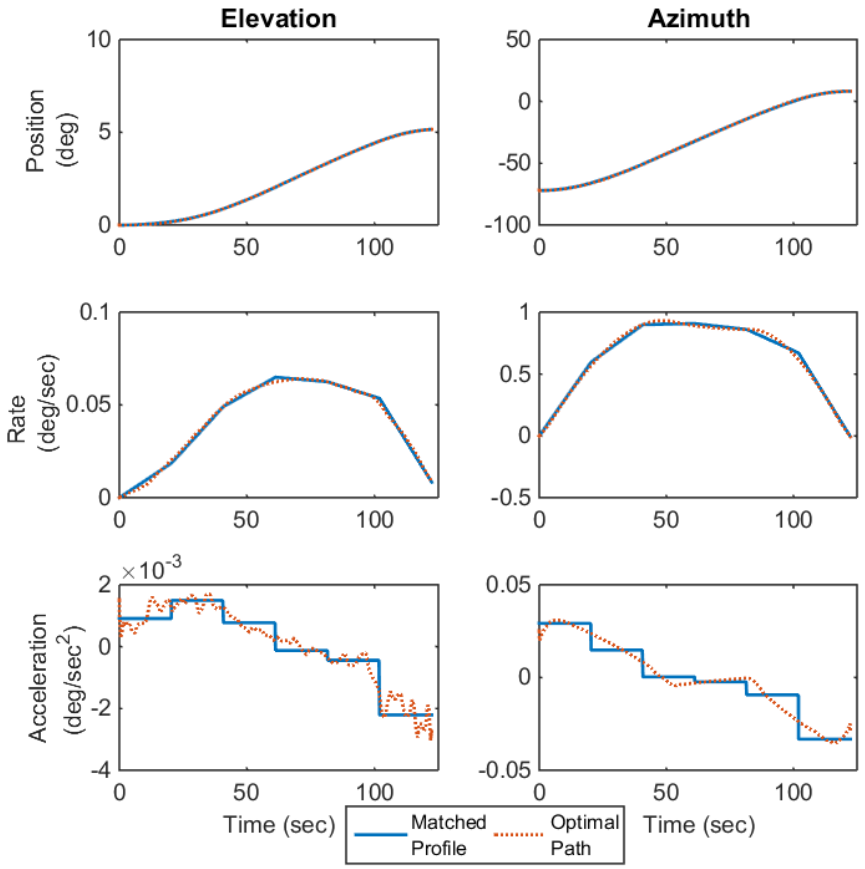

Figure 41. Matched profile with optimal path for scenario six with $N = 3$.

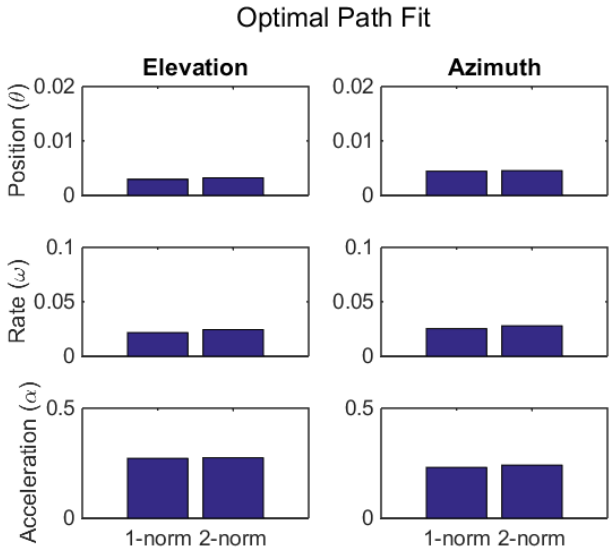

Figure 42. Fit error values of elevation and azimuth for scenario six with $N = 3$.

Finally, the graphs of simulation results with the optimal path for $N = 4$ are presented in Figure 43. This case provides a very small improvement over the $N = 3$ case and it is hard to see any obvious different in the graphical results.

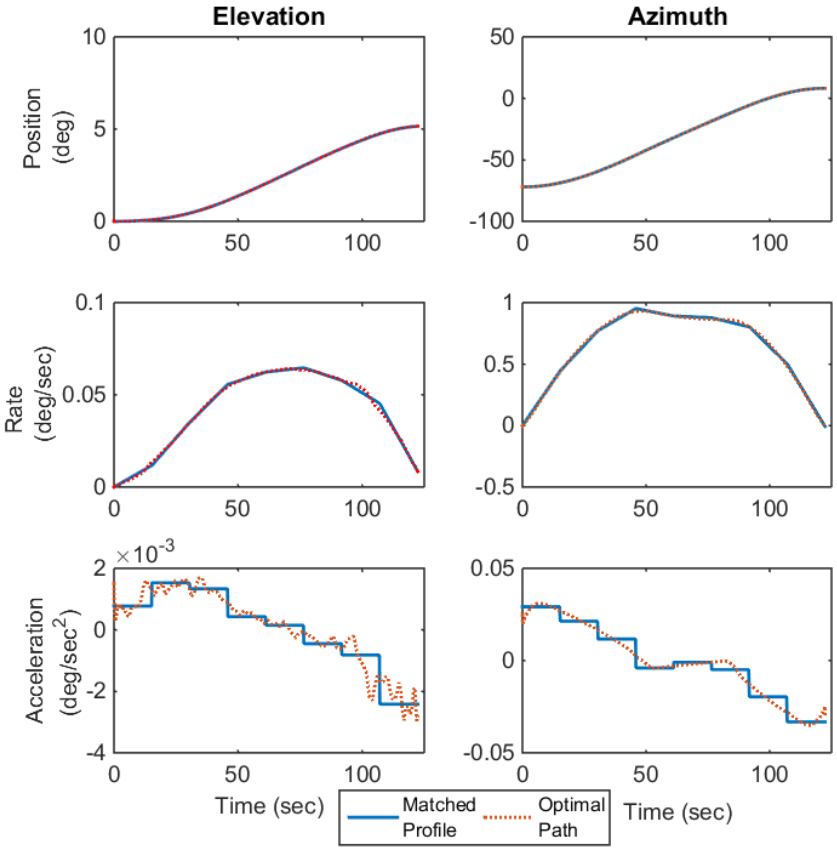

Figure 43. Matched profile with optimal path for scenario six with $N = 4$.

For this scenario, the position error has been maintained at less than 0.5% for both axes. This result shows a small improvement over the $N = 3$ case but not a major jump in terms of error reduction. Figure 44 presents the resulting error norm values for this case.

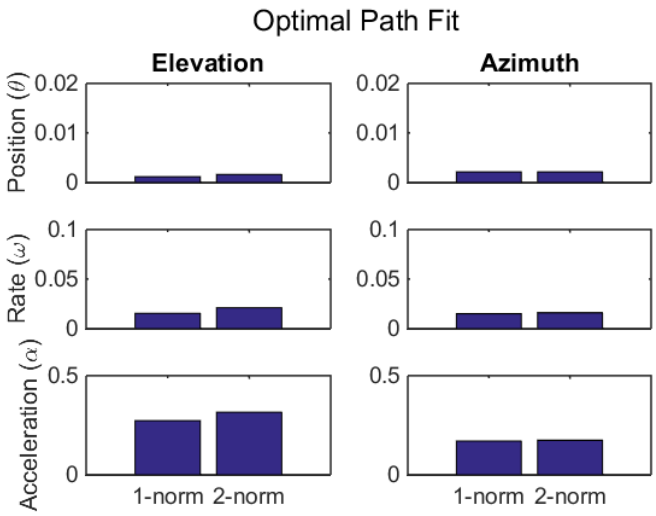

Figure 44. Fit error values of elevation and azimuth for scenario six with $N = 4$.

D. SUMMARY

Current maneuver planning methods used on TDRS are based solely on kinematics and reduce potential user access time. As presented in this chapter, TDRS has the potential for improving its capacity through the implementation of optimal antenna slews. The use of optimal slew paths presents the challenges discussed throughout this thesis. TDRS represents a good candidate for testing the optimal path implementation described in this thesis. The test cases developed in [1] were matched using the model developed with positive results. In all cases, the optimal minimum time was attained using the path matching technique.

Overall the results of this chapter demonstrate that a trade space exists for implementation of the developed technique. The step sensitivity analysis performed on scenario six demonstrates that a point of diminishing returns will be reached where the addition of steps does not produce sufficient benefit to be of use. Each situation is different and the mission will determine the error threshold required. Performance improvement must be balanced against the potential complications from adding steps.

THIS PAGE INTENTIONALLY LEFT BLANK

VII. CONCLUSIONS AND FUTURE WORK

A. CONCLUSIONS

This thesis demonstrates an approach for implementing an optimal control solution using current kinematics based control techniques. A sequence of standard maneuvers can be employed to closely match a reference pointing profile. The first variation of the idea, representing the lower bound of comparison, employed rest-to-rest steps to match the desired profile. While this method was capable of generating the shape of the desired reference path, it required additional time to execute the maneuver. This prevents the approach from being used in most applications, where system nonlinearities and dynamic coupling are used to enhance performance.

To improve maneuver times, a more sophisticated model was developed that incorporated the use of non-rest steps. This allowed the system to maintain the advantage of dynamic coupling between constituent bodies that is the basis of the optimal control advantage. This approach matched reference profiles while preserving the majority of performance improvement from optimal control results without requiring additional time to complete the maneuver. Further, sensitivity analysis showed that many cases can be matched to reasonable levels using only a few intermediate steps. In all cases tested, the resulting position error between the matched maneuver and the optimal reference path was less than 2% for fewer than five steps. Reducing the number of steps is an important operational consideration since many systems are not designed to perform optimal maneuvers.

Finally, the method developed was applied to an operational satellite system, TDRS, based on previously determined optimal paths. The non-rest matching method reproduced all optimal paths tested to position errors less than 0.5% using fewer than three steps. This demonstrates that, in theory, an optimal trajectory can be implemented on an existing system without major changes in system processing to accommodate polynomial trajectories. It is also possible that new system designs can be simplified,

yielding a cost reduction, based on the fact that simple maneuver segments could be used to achieve more complex optimal paths.

The approach for re-creating optimal paths using an existing control system is not unique to satellite antenna pointing systems. The approach also has potential application in robotics and optics. In general, this process can be applied to any system involving a multiplicity of gimbaled joints.

B. FUTURE WORK

This thesis was limited to the investigation of the feasibility of implementation of optimal control paths using currently implemented methods. Numerous control implementations exist and are based on the user requirements and operational limits of the system. This thesis only considers the simplest case (prevalent in industry) where users can turn torque on and off. Other types of input shaping may produce different results and should be investigated.

This work only considered reproducing the reference optimal trajectory. In many applications, the vibration effects may be of concern and the additional applications of control torque may induce undesirable motion in the system. The TDRS case optimal reference path was designed to minimize these disturbances but is based on having the ability to vary acceleration. The effects of step transitions in acceleration modeled were not included in that analysis. Further analysis as well as numerical simulation should be performed to fully investigate these effects.

Two operational areas of interest are also related to this research. First, a cost estimate of implementation should be developed. This study should include the cost of required software or personnel changes, as well as consideration of potential savings from added capacity resulting from more efficient maneuvers. Second, the best use of added capacity resulting from this work should be considered. Capacity gained could be used to serve additional customers or could be held as a surge element for high volume periods or casualty situations.

Finally, this work has been based purely in theory and simulation. Practical implementation on a test bed or physical system would also provide valuable data. Experimental results would further validate the approach developed in this thesis and could provide further insight at the hardware level.

THIS PAGE INTENTIONALLY LEFT BLANK

LIST OF REFERENCES

[1] A. G. Sears, "Design and experimental implementation of optimal spacecraft antenna slews," M.Sc. thesis, MAE Dept., Naval Postgraduate School, Monterey, CA, 2013.

[2] M. Karpenko, et al., "First flight results on time optimal spacecraft slews," *J. of Guidance, Control, and Dynamics*, vol. 35, no. 2, pp. 367–376, Mar-Apr. 2012.

[3] I. M. Ross, *A Beginner's Guide to DIDO*, Monterey, CA: Ellisar, LLC, 1998–2007.

[4] I. M. Ross and M. Karpenko, "A review of pseudospectral optimal control: From theory to flight," *Annu. Rev. of Control*, vol. 36, no. 2, pp. 182–197, Dec. 2012.

[5] K. D. Bilimoria and B. Wie, "Time-optimal three-axis reorientation of a rigid spacecraft," *J. of Guidance, Control, and Dynamics*, vol. 16, no. 3, pp. 446–452, May-Jun. 1993.

[6] B. Bishop et al., "Rapid maneuvering of multi-body dynamic systems with motion compensation," presented at AIAA/AAS Astrodynamics Specialist Conf., San Diego, 2014.

[7] R. P. Agrawal and D. O'Regan, *Ordinary and Partial Differential Equations*, New York, NY, Springer Science+Business Media, LLC, 2009, lecture 14, pp. 104–108.

[8] I. M. Ross, *A Primer on Pontryagin's Principle in Optimal Control*, Carmel, CA: Collegiate Publishers, 2009.

[9] M. R. Osbourne, "On shooting methods for boundary value problems," *J. of Math. Anal. and Appl.*, vol. 27, pp. 417–433, 1969.

[10] L. F. Shampine, J. Kierzenka, and M. W. Reichelt, (2000, Oct.). Solving boundary value problems for ordinary differential equations in MATLAB with bvp4c. MathWorks, Inc. Natick, MA. [Online]. Available: http://www.mathworks.com/matlabcentral/fileexchange/3819-tutorial-on-solving-bvps-with-bvp4c

[11] R. D. Russell and L. F. Shampine, "A collocation method for boundary value problems," *Numer. Math.*, vol. 19, no. 1, pp. 1–28, 1972.

[12] H. Maurer and N. P. Osmolovskii, "Second order sufficient conditions for time-optimal bang-bang control," *SIAM J. on Control and Optimization.*, vol. 42, no. 6, pp. 2239–2263, 2004.

[13] F. L. Lewis, D. M. Dawson, and C. T. Abdallah, *Robot Manipulator Control: Theory and Practice, Revised and Expanded*, 2nd ed. New York, NY: Marcel Dekker, 2004.

[14] E. Stoneking, "Newton-Euler dynamic equations of motion for a multi-body spacecraft," presented at AIAA Guidance, Navigation, and Control Conf., Hilton Head, SC, 2007.

[15] B. Ekstrand, "Equations of motion for a two-axes gimbal system," *IEEE Transactions on Aerospace and Electronic Systems*, vol. 28, no. 4, pp. 1083–1091, Apr. 2001.

[16] H. Schmeichel and T. McElroy, "TDRSS Single-Access Antenna Control System," in *Guidance and Control 1980*, vol. 42, *Advances in the Astronautical Sciences*, L. A. Louis, Ed., San Diego: Published for the American Astronautical Society by Univelt, inc., 1980, pp. 115–146.

[17] Tutorial #1: An introduction to Matlab/Simulink. (n.d.). University of Waterloo, Department of Mechanical and Mechatronics Engineering. [Online]. Available: http://mme.uwaterloo.ca/~mte360/Tutorial01_matlabsimulink.pdf. Accessed Jun. 10, 2014.

[18] E. Todorov, "Optimal control theory," in *Bayesian brain: probabilistic approaches to neural coding*, K. Doya, Ed., Cambridge, MA: MIT Press, 2006, pp. 269–298.

[19] M. Karpenko. (2014, August). MATLAB function: fixed_ISM_new.m, unpublished.

[20] L. N. Trefethen and D. Bau, *Numerical Linear Algebra*, Philadelphia, PA: Society for Industrial and Applied Mathematics, 1997, lecture 3 & 4, pp. 17–31.

[21] J. Yuan, D. Yang, X. Sun, "Single access antenna pointing control system design of TDRS," in *1st Int. Symp. on Syst. and Control in Aerospace and Astronautics*, Harbin, China, 2006, pp. 1093–1097.

[22] Q. Tham et al., "Robust antenna pointing control for TDRS spacecraft," in *Proc. of the 36th Conf. on Decision & Control*, San Diego, CA, 1997, vol. 5, pp. 4938–4942.

INITIAL DISTRIBUTION LIST

1. Defense Technical Information Center
   Ft. Belvoir, Virginia

2. Dudley Knox Library
   Naval Postgraduate School
   Monterey, California